

Universal link between polymer and glass physics inferred from double glass transitions in small-molecule liquids

Ben A. Russell,¹ Nikita V. Tukachev,¹ Mario González-Jiménez,¹ Laure-Anne Hayes,¹ Tajrian Chowdhury,¹ Uroš Javornik,² Gregor Mali,³ Joy H. Farnaby,¹ Manlio Tassieri,⁴ Hans M. Senn,¹ Klaas Wynne^{1*}

¹School of Chemistry, University of Glasgow, UK

²Slovenian NMR Centre, National Institute of Chemistry, Ljubljana, Slovenia

³Department of Inorganic Chemistry and Technology, National Institute of Chemistry, Ljubljana, Slovenia

⁴Division of Biomedical Engineering, School of Engineering, University of Glasgow, UK

At the glass transition, a supercooled liquid vitrifies into an amorphous solid and all viscous relaxation processes cease.¹ The experimental observation of secondary or β relaxations below the glass transition temperature in molecular and metallic glasses^{2,3} suggests that this picture may be somewhat oversimplified but essentially correct. Polymers, on the other hand, are thought of as fundamentally different: on cooling, polymers typically show a cascade of transitions from a viscous liquid, through viscoelastic fluid and viscoelastic solid stages, and finally a brittle glass.⁴ Here we show that a family of homogeneous non-polymeric liquids—titanium tetraalkoxides—have double glass transitions giving rise to two distinct steps in the temperature-dependent heat capacities. The double glass transition causes the liquid to transition from viscous to viscoelastic to elastic, like a simple polymer liquid. This result allows us to link the physical behaviour of polymers and small-molecule glass formers in a single universal picture.

Introduction

A glass transition is the kinetic arrest or the freezing out of a diffusive degree of freedom. Translational and rotational molecular diffusion rates are inversely proportional to the macroscopic shear viscosity constituting the primary or α relaxation, with small deviations caused by the inhomogeneous nature of the glassy state. The viscosity (η) becomes extremely high (typically defined as $\eta \sim 10^{12}$ Pa·s when the primary relaxation time is about 100 s) at a temperature very close to the glass transition temperature (T_g) defined as the temperature at which the heat capacity shows a steep drop in value. As the molecular diffusion and viscosity are intimately tied up, one expects to observe only one glass transition.

Second glass transitions have been seen in binary glass forming systems such as methyltetrahydrofuran with tristyrene,⁵ tripropyl phosphate with polystyrene,⁶ and aqueous citric acid,⁷ and even a triple glass transition the fluoroaluminosilicate Fuji G338 ionomer glass system.⁸ However, in these mixtures the multiple glass transitions are associated with inhomogeneities and the vitrification of chemically distinct components of the mixture. A slightly different example is the apparent double glass transition observed in some polymers caused by the emergence of partial crystallinity (for example, in polyethylene).⁹ Finally, a double glass transition associated with a liquid–liquid transition has been observed in yttrium-aluminium oxide glasses.^{10,11}

Many glass formers show secondary or β -relaxations, which appear at temperatures below the glass transition and are faster than the primary relaxation. These are often considered to play a minor role in vitrification as they

typically involve small angle orientational diffusion of the side chains or functional groups in polymers.^{12,13} The observation of β relaxations in rigid molecular glass formers and even metallic glasses^{2,3} shows that some of these may have an intermolecular character. Either way, secondary relaxations make a minor contribution to changes in heat capacity and dielectric relaxation.

Here we show that homogeneous (pure) non-polymeric titanium alkoxide liquids exhibit two calorimetric glass transitions. In addition, these liquids exhibit an extensive viscoelastic range and what appears to be a rubber plateau normally only associated with polymers. The high-temperature calorimetric transition is a glass transition in the classic sense associated with the freezing out of whole-molecule translational motion (classic primary or α relaxation). We find that below the glass transition, diffusive translational motion is made possible by extensive isomerisation of the molecules. This secondary relaxation process freezes out at the low-temperature glass transition, which has a similar or even greater magnitude (change in heat capacity) than the high-temperature one. This unique behaviour is conceptually in between that of small-molecule and polymeric glass formers and illustrates the fundamental connection between the two. It is applicable to the vitrification of any molecular or atomic liquid that allows intra- or intermolecular isomerisation such as glass-forming network liquids including water.

Results

The alkoxides. A number of alkoxides based on silicon, niobium, and titanium were studied here (see Fig. 1).

Silicon tetraalkoxides are monomeric in both liquid and crystalline phases. Short chain silicon alkoxides can crystallise while longer chain ones (*e.g.*, silicon tetrabutoxide) only vitrify into a glass and were recently studied to understand the emergence of the boson peak in molecular glasses.¹⁴ Pentaalkoxides based on niobium and tantalum are typically six-coordinated, dimeric in both liquid and crystalline phases, and bioctahedral.

Titanium-based tetraalkoxides tend to form oligomeric clusters with (imperfect, see below) octahedral and trigonal bipyramidal symmetry. The titanium alkoxides are tetrameric when a crystal can form (methoxide and ethoxide),^{15,16} monomeric when there is significant steric hindrance (*e.g.*, isopropoxide), and trimeric in the typical liquid.¹⁷ Titanium alkoxides with propoxide or longer chains do not crystallise at all and are therefore “perfect” glass formers in that sense. All the alkoxides studied here are liquid at room temperature and do not crystallise during the experiments.

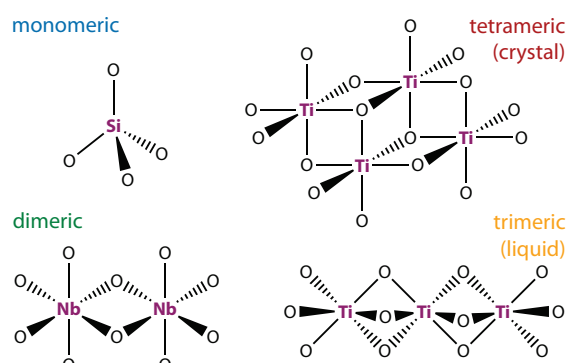


Fig. 1. Cartoon structures of three transition-metal alkoxides. Only the oxygen atoms of the alkoxide groups are shown here. Silicon alkoxides have the formula $\text{Si}(\text{OR})_4$, silicon prefers tetrahedral coordination, and is therefore monomeric in the liquid and crystal. Niobium alkoxides have the formula $\text{Nb}(\text{OR})_5$, niobium prefers octahedral coordination, and is therefore dimeric in the liquid and crystal. Titanium alkoxides have the formula $\text{Ti}(\text{OR})_4$, while titanium prefers octahedral coordination. Due to steric hindrance, these typically form trimers in the liquid. If the alkoxide is short (methoxide and ethoxide), it can crystallise in the tetrameric form.

Two calorimetric glass transitions. Monomeric silicon tetrabutoxide has a (single) calorimetric glass transition at $T_g = 120 \text{ K}$ ¹⁴ and other silicon alkoxides also behave as expected. In contrast, trimeric titanium alkoxides show two glass transitions (see Fig. 2) clearly identifiable by step changes in the isobaric heat capacity. The low-temperature transition is in all cases at $T_{g1} \approx 175 \text{ K}$ (-100°C), varying slightly ($\pm 15 \text{ K}$) with alkoxide chain length. The high-temperature transition is observed at $T_{g2} \approx 230 \text{ K}$ (-40°C), again varying slightly ($\pm 5 \text{ K}$) with alkoxide chain length (see Supplementary Table 1 and Supplementary Table 2). The high-temperature transition (which could be studied using controlled cooling and heating) shows the characteristic smooth transition on cooling. Both glass transitions show an overshoot on heating characteristic of a fragile glass former.^{18,19} All the trimeric titanium alkoxides show a bump in the heat capacity $\sim 15 \text{ K}$ above T_{g2} , which in previous work has been associated with a liquid–liquid transition.^{20,21}

To determine if the multiple glass transitions are caused by the non-monomeric nature of the titanium alkoxides,

niobium ethoxide and butoxide were investigated. While the former crystallises, the latter has a normal (single) glass transition. Similarly, monomeric titanium 2-ethylhexanoate also has a single glass transition. Thus, the unusual double glass transitions are only observed in trimeric alkoxides.

The changes in heat capacity at each glass transition are surprisingly large (ΔC_{p1} and ΔC_{p2} , see Supplementary Table 1 and Supplementary Table 2) ranging from 100 to $900 \text{ J K}^{-1} \text{ mol}^{-1}$ at each step. The expected value for ΔC_p in a simple model of non-spherical incompressible particle is $6R \approx 50 \text{ J K}^{-1} \text{ mol}^{-1}$,²² which is indeed observed for many small-molecule glass-forming liquids (for example, 1-propanol $\Delta C_p \approx 50 \text{ J K}^{-1} \text{ mol}^{-1}$, methylpentane 70,²³ 1-butanol 48,²⁴ toluene 60, and ethylbenzene 80²⁵). The comparatively large values of ΔC_p are only observed here for the trimeric titanium alkoxides. For example, monomeric silicon tetrabutoxide has $\Delta C_p = 206 \text{ J/K/mol}$ at its (single) glass transition¹⁴ similar to monomeric titanium 2-ethylhexanoate (142) and dimeric niobium butoxide (261).

A heat-capacity step at the glass transition much larger than $6R$ implies the freezing out of additional intramolecular diffusive motions or alternatively can be related to the thermal expansion coefficient and bulk modulus.²⁶ One may speculate that (in addition to translations and rotations) low-frequency (overdamped) vibrations such as alkoxide librations and torsions contribute to the ΔC_p .

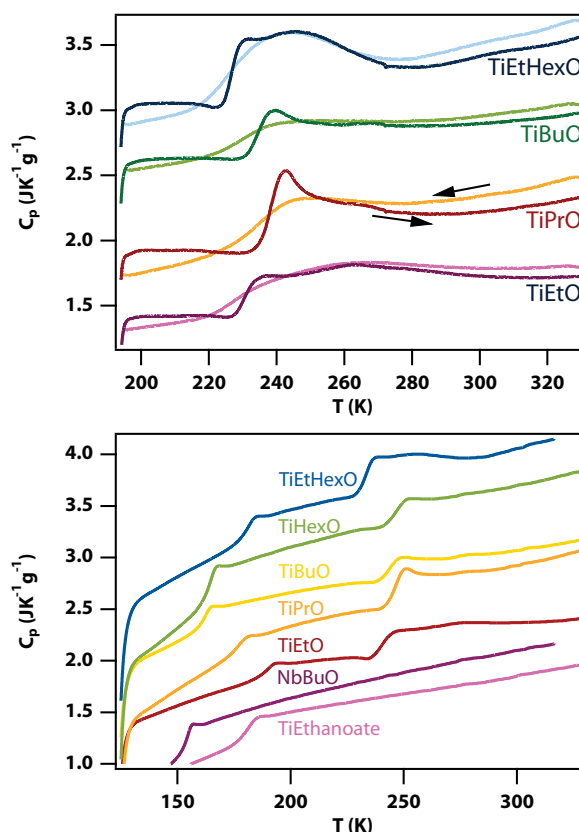


Fig. 2. Calorimetry of titanium-based alkoxides shows two calorimetric glass transitions. Heat capacity measurements of titanium ethoxide, propoxide, butoxide, hexoxide, 2-ethylhexoxide, and 2-ethylhexanoate as well as niobium butoxide. (**top**) Data obtained using controlled cooling to $\sim 190 \text{ K}$ and heating both at 10 K/min . See also Supplementary Table 1. (**bottom**) Data obtained using quench cooling with liquid nitrogen to $\sim 120 \text{ K}$ and heating at 20 K/min . See also

Supplementary Table 2. Curves have been shifted vertically for improved visibility.

Eliminating partial crystallisation as the cause for the double glass transition. Considering that in titanium alkoxides the coordination is different between the liquid and the crystal, it is imperative to determine that the glass transitions are not associated with simple coordination changes or partial crystallisation events.

Stretch and bend modes associated with the Ti-O-R motif are observed in the Raman spectrum between 500 and 1,500 cm^{-1} . In crystalline titanium methoxide, the titanium atom is octahedrally coordinated resulting in a very simple spectrum in the fingerprint region (see Supplementary Figure 1). This is in contrast to the much more complex spectra of titanium butoxide and 2-ethylhexyloxide. Temperature-dependent Raman spectra of the latter two taken throughout the liquid and glassy range show no spectral changes beyond line narrowing on cooling, demonstrating the absence of titanium coordination changes (Supplementary Figure 2 and Supplementary Figure 3).

Stretch modes associated with CH bonds are observed around 2,900 cm^{-1} . Subtle changes in the position and amplitudes of these peaks are associated with a transformation from a mixture of trans and gauche orientations at high temperature to predominantly trans alkoxide at low temperature.²⁷ This transformation is gradual and does not show steps near the glass transitions.

The temperature-dependent low-frequency Raman spectra of titanium 2-ethylhexyloxide, acquired using the femtosecond optical Kerr-effect technique (see Supplementary Figure 4),^{14,21} show collision-induced bands at 1.08 ± 0.05 THz and 1.8 ± 0.2 THz with a Lorentzian lineshape. This is similar to the Gaussian bands recently observed in silicon tetrabutoxide and identified as a boson peak combined with a peak due to acoustic phonons at the pseudo-Brillouin-zone edge. The difference in lineshape can be ascribed to the trimeric nature of the titanium alkoxides. Crucially, these low frequency Raman spectra do not show any phonon bands associated with crystallisation.

Rheology. The reduction in the heat capacity at the calorimetric glass transition, is always associated with a dramatic slowdown of the primary relaxation and hence a dramatic increase in the viscosity.²⁸ Given that the titanium alkoxides have two glass transitions, it is of the utmost importance to relate these to changes in the rheological behaviour.

The shear viscosities of titanium propoxide, butoxide, hexoxide, and 2-ethylhexyloxide as well as niobium butoxide were measured from 313 K (+40°C) down to a few K above their T_{g1} (see Fig. 3 and Supplementary Figure 5). The data were fitted with a Vogel-Fulcher-Tammann (VFT) expression $\eta(T) = \eta_0 \exp(D/(T - T_0))$, where T_0 is the temperature of apparent divergence of the viscosity.²⁸ However, none of the viscosities for trimeric alkoxides can be fully modelled by a single VFT function as all show a clear switch in behaviour around 230 K. High quality fits could be obtained by fitting the low-temperature range ($T_{g1} + 10$ K to 210 K) and high-temperature range (240 K to 300 K) separately (see Supplementary Table 3 for fit parameters). In all cases, $D > T_0$, consistent with these liquids being moderately fragile glass formers.¹ The T_0 parameters are in all cases ~ 10 -60 K below the respective calorimetric

T_g , i.e., both for the low (~ 175 K) and the high (~ 230 K) glass transitions also as expected for glass formers with moderate fragility. In contrast to the trimeric alkoxides, the measured shear viscosity of dimeric niobium butoxide and monomeric titanium 2-ethylhexanoate could be fit well with a single VFT expression as expected.

Temperature-dependent storage and loss moduli were measured using oscillatory rheology for titanium butoxide and titanium 2-ethylhexyloxide. The dynamic viscosity calculated from these is consistent with the shear viscosity. Both plateau near T_{g1} , with the maximum value determined by the frequency of rotation or oscillation as expected.

On cooling the liquid from room temperature, the loss tangent drops from very large ($\geq \sim 10^2$ - 10^3 for $T > T_{g2}$) to very small ($\leq 10^{-2}$ for $T < T_{g1}$) values showing a transition from viscous to elastic. Remarkably, the loss tangent values are intermediate—showing the liquids are viscoelastic—for $T_{g1} < T < T_{g2}$, a range of 50-80 K. Viscoelastic behaviour over such a large temperature range has never been observed in small molecule glass formers but is common in polymers where it is referred to as the rubbery plateau.⁴

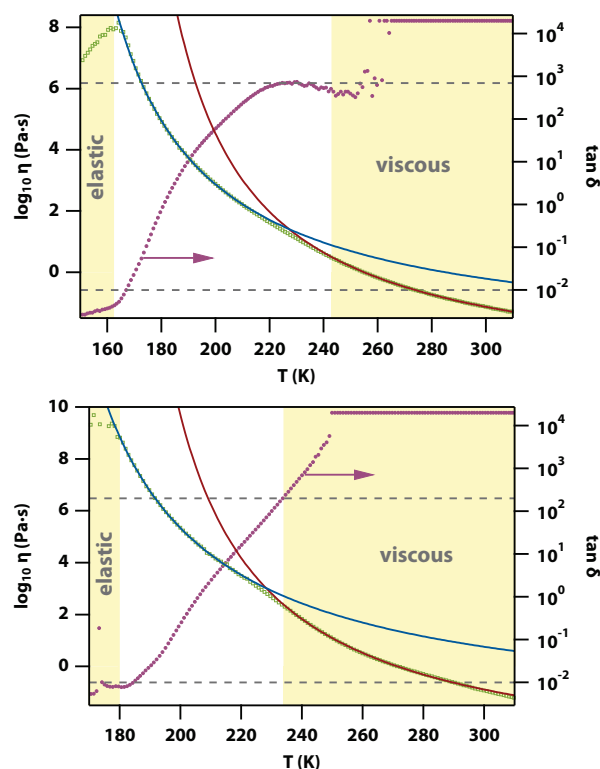


Fig. 3. Viscosity measurements of titanium butoxide and titanium 2-ethylhexyloxide. Shear viscosity up to a maximum of circa 10^{10} Pa.s (green circles) for titanium butoxide (top) and titanium 2-ethylhexyloxide (bottom). The lines are the fits of two separate Vogel-Fulcher-Tammann (VFT) expressions (blue and red lines, parameters in Supplementary Table 3). The regions $T < T_{g1}$, $T_{g1} < T < T_{g2}$, and $T > T_{g2}$ have been indicated by yellow, white, and yellow boxes. The right axis shows the loss tangent.

Isomerisation dynamics and self-diffusion. Earlier studies of transition metal alkoxides have reported “rapid” exchange of terminal and bridging alkoxides.²⁹ To establish the temperature-dependent rate of isomerisation through ligand exchange, ^{13}C magic-angle spinning (MAS) solid-state NMR was carried out on titanium ethoxide (Fig. 4 and

Supplementary Figure 6) and titanium 2-ethylhexyloxide (Supplementary Figure 7 and Supplementary Figure 8). As the former gave the cleanest spectra, we will concentrate on these.

The ^{13}C MAS NMR spectrum of titanium ethoxide shows lines at ~ 70 ppm due to the CH_2 group next to the oxygen atom and at ~ 20 ppm due to the terminal CH_3 group. At low temperature, both are split into multiple lines due to the presence of multiple isomers. At higher temperature these coalesce into single lines due to fast exchange on the NMR timescale.

This coalescence was modelled with a Bloch-McConnell exchange model with the temperature-dependent ligand exchange described by an Eyring equation with as the only free parameter the activation energy (see Supplementary note 1). This describes the data well for an activation energy of 52.3 kJ/mol for titanium ethoxide (see Fig. 4) and an activation energy of 46 ± 2 kJ/mol for titanium 2-ethylhexyloxide (see Supplementary Figure 8).

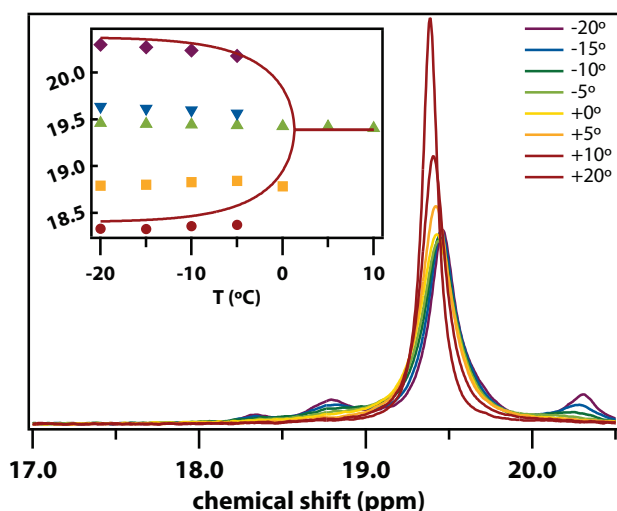


Fig. 4. ^{13}C MAS NMR spectra of titanium ethoxide in the region of the terminal CH_3 groups. Shown are spectra taken between -20° and 20°C . (inset) Temperature-dependent peak positions and Bloch-McConnell modelling of the line positions using an activation energy of 52.3 kJ/mol.

Transitions states and isomerisation. The calorimetry data show that the double glass transition only occurs in trimeric titanium alkoxides but not in dimeric or monomeric equivalents. This suggests an additional quality that is only present in these trimers.

Quantum chemistry calculations were carried out to establish which trimeric isomers were most likely to be present in the liquid (see Supplementary note 2). Out of a large range of trial structures, five isomers were found to be stable (see Fig. 5). For isomers I-III, the coordination number of each titanium atom is six, while the other structures have one or two titanium atoms with a coordination of five. None of the TiO_6 and TiO_5 coordination geometries are perfectly octahedral nor trigonal-bipyramidal or square-pyramidal, respectively, but are notably distorted. Isomers I, IV, and V are essentially linear whereas II and III are notably bent.

As can be seen in Supplementary Table 4, the energy differences between the isomers ranges from 2.5 to 32 kJ/mol and the most stable isomer is either II or III depending on the length of the alkoxide used (both II and III

are bent but the near-linear isomer IV is not much higher in energy).

The barriers for isomerisation between the five isomers identified were calculated (for a single titanium ethoxide trimer, see Supplementary note 3). Unsurprisingly, the barriers for isomerisation between linear isomers are low (33–68 kJ/mol) and those for isomerisation between bent isomers are also low (22–25 kJ/mol). Barriers for isomerisation from bent to linear are higher (74–135 kJ/mol). These values are clearly approximate and would likely be lower if each trimer could interact with neighbouring trimers, but such calculations are too expensive at present. Thus, the value of the barrier for linear to bent isomerisation is broadly consistent with the value found from the ^{13}C MAS NMR data.

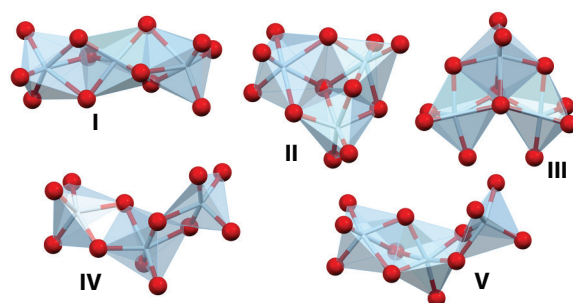


Fig. 5. Molecular models of the isomeric titanium alkoxide trimeric clusters in the liquid. DFT calculations show that these five clusters have similar energies, with the lowest-energy isomer dependent on the alkoxide chain length.

Discussion and conclusions

Here we have shown that titanium alkoxide liquids exhibit two calorimetric glass transitions with the transition temperatures weakly dependent on the length of the alkoxide chain (2 to 8 carbon atoms). Temperature-dependent Raman spectroscopy shows that these transitions are not related to any changes in the coordination of the titanium atoms, ruling out partial crystallisation. Rheology shows that, on cooling from room temperature, the shear viscosity increases in a VFT-like fashion down to T_{g2} and then continues to rise in a different VFT-like fashion down to T_{g1} . This is associated with transitions from viscous (liquid like) to viscoelastic (rubbery) to elastic (brittle glass). Neither the extra glass transition nor the unusual rheological behaviour are observed in monomeric (*e.g.*, silicon)¹⁴ or dimeric (niobium) alkoxides. This shows that the unusual behaviour is not related to the alkoxide side chains, but due to the trimeric nature of the titanium alkoxides.

Calculations show that the trimeric alkoxides are different from the monomeric and dimeric ones in that they can isomerise between five low-energy isomers. Solid-state NMR measurements show multiple lines coalescing into a single line at high temperature due to rapid isomerisation. This allowed us to model the isomerisation rate as an activated process with an activation energy of 46–52 kJ/mol. The calculations confirm that isomerisation can occur between linear and bent isomers with a comparable activation energy.

The isomerisation rate is plotted in Fig. 6 over the entire relevant temperature range through extrapolation. To understand the relevance of this rate, it is compared to the rate, k_{trans} , for one molecule (a titanium trimer) to diffuse

over a distance of one molecular diameter. In Fig. 6, this translational rate is plotted by using the experimentally measured viscosity. The rates of translation and isomerisation meet at 237 K just a bit above T_{g2} .

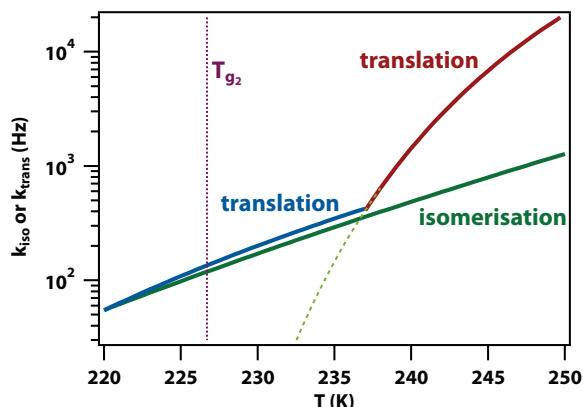


Fig. 6. The isomerisation rate crosses the translation rate at the high-temperature glass transition. Shown is the rate of isomerisation calculated with an Eyring equation using an activation energy of 46 kJ/mol appropriate for titanium 2-ethylhexyloxide (green). Also shown are the translational relaxation rates based on the VFT fits (see Supplementary Table 2) to the experimental shear viscosity of titanium 2-ethylhexyloxide for the low (blue) and high (red) temperature regions. The translational rate is calculated using the Stokes-Einstein and Fick laws and is given by $k_{trans} = k_B T / (d^3 \pi \eta)$, where η is the temperature-dependent viscosity and d the molecular diameter obtained from the liquid density.

The rapid drop of the loss tangent on cooling through T_{g2} —associated with a transformation from viscous to viscoelastic—demonstrates that the high-temperature glass transition is associated with the freezing out of the whole-molecule translational diffusion. In normal small-molecule glass formers, this would be referred to as “the glass transition” where the primary or α -relaxation freezes out.

However, in the case of the trimeric titanium alkoxides, a secondary relaxation channel is still available: isomerisation. At the temperature at which the rate of isomerisation overtakes the rate of translation, the viscosity will become dominated by isomerisation and the liquid becomes viscoelastic. This behaviour is similar to what polymer physics refers to as the “rubbery transition” but is seen here for the first time in a non-polymeric liquid.

It is found that the viscosity below T_{g2} increases in a VFT-like fashion with a T_0 just below the low-temperature calorimetric glass transition at T_{g1} . This implies that the dissipation of shear through isomerisation also has collective aspects resulting in the freezing out at a finite temperature. In polymer physics, this would be referred to, confusingly, as “the glass transition”.

The double glass transitions observed here rely on the isomerisation between linear and bent isomers. It is therefore expected that this effect will be of much wider relevance in, for example, glass-forming network liquids that allow for isomerisation such as amorphous quartz, silicon, and germanium.^{30,31} Relatively strong intermolecular hydrogen bonds could fulfil a similar role to the relatively weak covalent Ti-O bonds in, for example, water or N-methyl acetamide. In the latter, a change in the slope of the measured temperature-dependent orientational-diffusion

dynamics³² was assigned to the breakup of hydrogen-bonded molecular chains suggesting a similar effect at work.³³ The rheological observations made here are also reminiscent of the fragile-to-strong transition observed in liquid water.³⁴

The fields of glass and polymer physics appear disparate at present. What we refer to here as T_{g1} would be called the “glass transition” in polymer physics and a “shadow glass transition” or “sub- T_g endotherm” in metallic-glass physics.^{3,19,35} However, the effect has no known counterpart in small-molecule glass formers. It comes closest to secondary or β -relaxations, but these have never been seen to give rise to a distinct second glass transition either calorimetrically, rheologically, or spectroscopically. What we refer to as T_{g2} would be called the “rubber transition” in polymer physics and the “glass transition” in glass physics. Most commonly studied molecular glass formers interact through van der Waals forces and as a result have relatively low glass transition temperatures (e.g., toluene at 117 K²⁵). Therefore, the freezing out of β relaxations (shadow glass transition) in small-molecule glass formers would simply not be observed because it occurs at temperatures inaccessible to standard calorimetry and rheology (< 77 K). Thus, perhaps the most important insight obtained here is that the trimeric alkoxides exhibit behaviour in between that of small molecules and polymers, thereby demonstrating that these are just extremes on a continuous spectrum.

Methods

Sample preparation. Liquid titanium(IV) ethoxide ($\geq 97\%$), propoxide (98%), butoxide ($\geq 97\%$), 2-ethylhexyloxide (95%), and tetrabutyl orthosilicate (97%), were purchased from Sigma-Aldrich while niobium n-butoxide (99%) and titanium(IV) 2-ethylhexanoate (97%) were purchased from Alfa Aesar and were used without further purification. Titanium hexoxide was synthesised as described in Supplementary note 4.

The alkoxides used here react slowly with water from the air: in seconds in the case of titanium ethoxide to hours in the case of monomeric and dimeric species. This reaction forms a film on the surface of the samples thereby sealing the sample. However, prolonged exposure does cause the formation of oxo-bridged polymeric molecules and the gradual disappearance of the multiple glass-transition effects described here. Therefore, the samples were stored and handled in a glovebox with a dry air atmosphere (dew point $< -40^\circ\text{C}$).

Differential scanning calorimetry. Differential scanning calorimetry (DSC) measurements were carried out with a TA Instruments DSC 2500 differential scanning calorimeter equipped with either a RCS90 cooling system allowing cooling to -90°C or a Quench Cooling Accessory allowing cooling from $+40^\circ\text{C}$ to about -165°C with liquid nitrogen in circa 16 minutes. Samples were prepared and DSC pans sealed in the dry-air glove box.

Raman. Confocal Raman microscopy experiments were performed using a Horiba LabRAM HR confocal microscope system. The excitation source was a linearly polarised 28-mW frequency-doubled DPSS laser operating at 532 nm. Temperature was controlled to ± 0.1 K using a Linkam THMS600 microscope stage. The samples were

prepared in the dry-air glove box and dispensed into a quartz crucible (18 mm diameter, 3 mm depth) then sealed with an 18 mm diameter cover slip and silicon grease.

OKE experimental details. A laser oscillator (Coherent Micra) produced ~ 10 nJ pulses at a repetition rate of 82 MHz and with 800 nm nominal wavelength providing 20 fs temporal pulse width in the sample, broadening to 25 fs when using a cryostat. The OKE data were recorded in a standard time-domain pump-probe configuration and Fourier transformed to obtain the frequency-domain reduced depolarised Raman spectrum as described previously.³⁶ The data were analysed through curve fitting as described previously.¹⁴

Rheology. Rheology measurements were carried out on an Anton Paar MCR 702e rheometer equipped with a CTD 600 MDR convection temperature device. The temperature-dependent shear viscosity was measured by using a 50-mm cone-plate geometry (cone angle = 1° , gap = 0.101 mm) or a 50-mm parallel-plate geometry (gap = 1 mm) using a shear rate of 0.3 rad/s allowing the viscosity to be measured down a few K above T_{g1} . The temperature-dependent storage ($G'(\omega)$) and loss moduli ($G''(\omega)$) were measured by using a 50-mm parallel-plate geometry and oscillation frequencies of either 1 or 10 Hz. These measurements were used to calculate the complex viscosity, $\eta^* = G(\omega)/\omega$, and hence the dynamic viscosity $\eta' = \text{Re } \eta^*$ in addition the loss tangent $\tan \delta = G''(\omega)/G'(\omega)$. The temperature was lowered from 30°C to -160°C at a rate of 1°C/min and the data recorded every minute.

As the alkoxide liquids react slowly with water from the air, a special procedure was used for sample loading. A home-made plastic and rubber cup was placed on the lower measuring plate forming a good seal. The cup was filled with xenon gas, which is heavier than air and therefore keeps the ambient air away from the lower measuring plate. A sample in a micropipette is prepared in the glove-box, transferred to the rheometer, and put on the xenon-covered lower measuring plate. A cone or parallel plate is then lowered through the gas onto the sample. The cup can then be lifted up and the CTD 600 MDR convection temperature device closed, which then flushes dry air through the sample chamber.

MAS NMR. Temperature-dependent ^{13}C magic-angle spinning (MAS) NMR spectra were recorded on a 400 MHz Bruker Avance Neo spectrometer equipped with a 4-mm Bruker CPMAS probe. The investigated liquids were closed into Kel-F inserts before being put into 4 mm zirconia rotors. These samples were prepared in an argon-filled (BOC, 99.998%) glove box (MBraun LABstar, $\text{O}_2 \leq 5$ ppm, $\text{H}_2\text{O} \leq 0.5$ ppm). In the MAS-NMR experiments, the samples were spun with a frequency of 10 kHz. A 90° pulse of 3.8 μs was used for the excitation of carbon nuclei, and proton decoupling was employed during signal acquisition. The number of scans was 256 using a repetition delay of 3 s and an acquisition to 540 ms to acquire 32k points. The processed data were apodised with 2.5 Hz LB exponential function and baseline corrected with a polynomial. The ^{13}C shifts are reported relative to the position of the ^{13}C signal of tetramethylsilane (TMS).

Isomer stability and normal mode calculations. All calculations were performed using the ORCA 5.0 quantum chemistry program.³⁷ A preliminary conformational search to find low-energy TiO skeletons for titanium alkoxides trimers was carried out using the semiempirical GFN2-xTB method.³⁸ Geometry optimisations and vibrational spectral calculations were carried out with the PBE exchange-correlation functional³⁹ with the Grimme dispersion correction (D3)⁴¹ with Becke-Johnson damping⁴² combined with def2-SVP basis set.⁴³ PBE is a nonempirical GGE functional applicable to a broad range of systems from simple organic molecules to inorganic solids and metals, while the def2-SVP basis set is known to provide a good trade-off between accuracy and cost. To estimate errors arising due to basis set incompleteness, calculations with triple-zeta (def2-TZVP, def2-TZVPP) basis sets were also performed. To validate the energy ordering of different titanium alkoxide trimers, PBE0-D3(BJ)/def2-TZVPP calculations (geometry optimisations starting with converged PBE-D3(BJ)/def2-SVP structures) were conducted. Solvent effects were accounted for throughout by using the CPCM polarisable continuum model⁴⁴ with a dielectric constant of $\epsilon_{\text{static}} = 1.89$ (hexane). For all DFT calculations, the RI approximation was employed.

It is known that titanium ethoxide and butoxide form trimers in neat liquid and solution (except at high dilution).^{45–47} In order to identify low-energy trimers, various Ti_3O_{12} cores were cut from crystal structures of rutile and anatase TiO_2 polymorphs, saturated with hydrogens, and optimised with the GFN2-xTB method, yielding four different isomers. Next, the hydrogens were substituted by methyl, ethyl, or butyl, and DFT optimisations were performed. Additional Ti_3O_{12} cores were obtained from $\text{Ti}(\text{OR})_4$ crystal structures from the Cambridge Structural Database. Their optimisation as $\text{Ti}_3(\text{OH})_{12}$ yielded one more stable isomer, thus leading to five different minima on the PES (see Fig. 5, Supplementary note 2, and Supplementary Figure 9). All geometry optimisations were performed without symmetry constraints. Ti_3O_{12} cores were found to be close to S_6 (**I**), C_2 (**III**, **IV**) and C_s (**II**, **V**) symmetry. Harmonic analyses of these structures showed that all Hessian eigenvalues are positive. The optimised structures **I–V** were compared to those proposed in the literature based on general considerations⁴⁷ or theoretical studies.¹⁷ Our structures **I** and **III** correspond to **I** and **II** of Refs.^{17,46}; structure **IV** is known from crystal trimers. However, it appears that structures **II** and **V** have not previously been considered. Structures **III** and **IV** of Ref.⁴⁷ are not stable and rearrange to one of the five stable isomers identified herein during geometry optimisation.

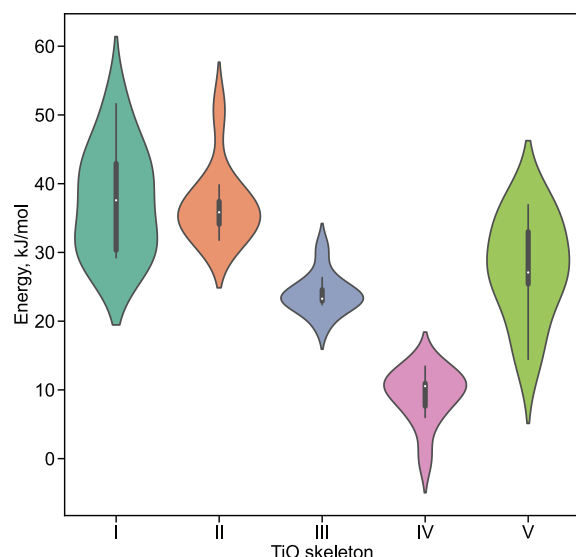


Fig. 7. Violin plots for conformer energy distributions for different TiO skeletons of $\text{Ti}(\text{OEt})_4$ trimers. Energies estimated by PBE0-D3(BJ)/def2-TZVP, CPCM(hexane)

Although a full conformational analysis of the alkyl chains in solution for all studied alkoxides was not carried out, it was decided to investigate conformer energy distributions for Ti ethoxide trimers (Fig. 7). For this purpose, 50 ps GFN2-XTB MD runs were conducted for each of the skeletons (NVT ensemble, Berendsen thermostat, 300 K, log-fermi potential to confine a trimer in a spherical cavity to prevent possible dissociation). Ten snapshots were then extracted from resulting trajectories and optimised with PBE0-D3(BJ)/def2-TZVP, CPCM (hexane) resulting in 50 DFT-optimised structures in total. For methoxides and butoxides, the optimised alkyl conformations are to some extent arbitrary; butyl chains have the all-trans “zig-zag” conformation. Enthalpies and Gibbs energies were estimated within the rigid rotator–harmonic oscillator model.

IR and depolarised Raman spectra were obtained in the double harmonic approximation; Raman data were converted to OKE spectra using a Bose-Einstein correction as described previously.¹⁴ Spectra were broadened with Lorentzians with a 12 cm^{-1} half-width (see Supplementary Figure 10 and Supplementary Figure 11).

Data availability

The data that support the findings of this study are available in Enlighten: Research Data Repository (University of Glasgow) with the identifier: <http://dx.doi.org/10.5525/gla.researchdata.@@@>.

References

- Angell, C. A., Ngai, K. L., McKenna, G. B., McMillan, P. F. & Martin, S. W. Relaxation in glassforming liquids and amorphous solids. *J. Appl. Phys.* **88**, 3113–3157 (2000).
- Hai Bin Yu, Wei Hua Wang, Hai Yang Bai, & Konrad Samwer. β -relaxation in metallic glasses | National Science Review | Oxford Academic. *Natl. Sci. Rev.* **1**, 429–461 (2014).
- Yang, Q., Peng, S.-X., Wang, Z. & Yu, H.-B. Shadow glass transition as a thermodynamic signature of β relaxation in hyper-quenched metallic glasses. *Natl. Sci. Rev.* **7**, 1896–1905 (2020).
- Ohring, M. Mechanical behavior of solids. in *Engineering Materials Science* (ed. Ohring, M.) 299–V (Academic Press, 1995). doi:10.1016/B978-012524995-9/50031-3.
- Blochowiec, T., Lusceac, S. A., Gutfreund, P., Schramm, S. & Stühn, B. Two Glass Transitions and Secondary Relaxations of Methyltetrahydrofuran in a Binary Mixture. *J. Phys. Chem. B* **115**, 1623–1637 (2011).
- Jin, X. *et al.* Experimental evidence of co-existence of equilibrium and nonequilibrium in two-glass-transition miscible mixtures. *Phys. Chem. Chem. Phys.* **22**, 25631–25637 (2020).
- Bogdan, A., Molina, M. J., Tenhu, H. & Loerting, T. Multiple Glass Transitions and Freezing Events of Aqueous Citric Acid. *J. Phys. Chem. A* **119**, 4515–4523 (2015).
- Tian, K. V. *et al.* Atomic and vibrational origins of mechanical toughness in bioactive cement during setting. *Nat. Commun.* **6**, 8631 (2015).
- Boyer, R. F. An apparent double glass transition in semicrystalline polymers. *J. Macromol. Sci. Part B* **8**, 503–537 (1973).
- Wilding, M. C. & McMillan, P. F. Polyamorphic transitions in yttria–alumina liquids. *J. Non-Cryst. Solids* **293–295**, 357–365 (2001).
- Wilding, M. C., McMillan, P. F. & Navrotsky, A. Thermodynamic and structural aspects of the polyamorphic transition in yttrium and other rare-earth aluminate liquids. *Phys. Stat. Mech. Its Appl.* **314**, 379–390 (2002).
- Ngai, K. L. & Paluch, M. Classification of secondary relaxation in glass-formers based on dynamic properties. *J. Chem. Phys.* **120**, 857–873 (2004).
- Kunal, K., Robertson, C. G., Pawlus, S., Hahn, S. F. & Sokolov, A. P. Role of Chemical Structure in Fragility of Polymers: A Qualitative Picture. *Macromolecules* **41**, 7232–7238 (2008).
- Mario Gonzalez-Jimenez *et al.* Understanding the emergence of the boson peak in molecular glasses. doi: [10.26434/chemrxiv-2022-25q9h](https://doi.org/10.26434/chemrxiv-2022-25q9h), (2022).
- Wright, D. A. & Williams, D. A. The crystal and molecular structure of titanium tetramethoxide. *Acta Crystallogr. B* **24**, 1107–1114 (1968).
- Ibers, J. A. Crystal and Molecular Structure of Titanium (IV) Ethoxide. *Nature* **197**, 686–687 (1963).
- Ignatyev, I. S., Montejo, M. & López González, J. J. DFT predictions of vibrational spectra of titanium tetramethoxide oligomers and the structure of titanium tetraalkoxides in liquid and solid phases. *Vib. Spectrosc.* **51**, 218–225 (2009).
- Angell, C. A. Liquid Fragility and the Glass Transition in Water and Aqueous Solutions. *Chem. Rev.* **102**, 2627–2650 (2002).
- Zheng, Q. *et al.* Understanding Glass through Differential Scanning Calorimetry. *Chem. Rev.* **119**, 7848–7939 (2019).
- Harris, M. A., Kinsey, T., Wagle, D. V., Baker, G. A. & Sangoro, J. Evidence of a liquid–liquid transition in a glass-forming ionic liquid. *Proc. Natl. Acad. Sci.* **118**, (2021).
- Walton, F. *et al.* Polyamorphism Mirrors Polymorphism in the Liquid–Liquid Transition of a Molecular Liquid. *J. Am. Chem. Soc.* **142**, 7591–7597 (2020).
- Ke, H. B., Wen, P. & Wang, W. H. The inquiry of liquids and glass transition by heat capacity. *AIP Adv.* **2**, 041404 (2012).
- Takahara, S., Yamamuro, O. & Suga, H. Heat capacities and glass transitions of 1-propanol and 3-methylpentane under pressure. New evidence for the entropy theory. *J. Non-Cryst. Solids* **171**, 259–270 (1994).
- Shmyt'ko, I. M., Jiménez-Riobóo, R. J., Hassaine, M. & Ramos, M. A. Structural and thermodynamic studies of n-butanol. *J. Phys. Condens. Matter* **22**, 195102 (2010).
- Yamamuro, O. *et al.* Calorimetric Study of Glassy and Liquid Toluene and Ethylbenzene: Thermodynamic Approach to Spatial Heterogeneity in Glass-Forming Molecular Liquids. *J. Phys. Chem. B* **102**, 1605–1609 (1998).
- Trachenko, K. & Brazhkin, V. V. Heat capacity at the glass transition. *Phys. Rev. B* **83**, 014201 (2011).

27. Weeraman, C., Yatawara, A. K., Bordenyuk, A. N. & Benderskii, A. V. Effect of Nanoscale Geometry on Molecular Conformation: Vibrational Sum-Frequency Generation of Alkanethiols on Gold Nanoparticles. *J. Am. Chem. Soc.* **128**, 14244–14245 (2006).
28. Hecksher, T., Nielsen, A. I., Olsen, N. B. & Dyre, J. C. Little evidence for dynamic divergences in ultraviscous molecular liquids. *Nat. Phys.* **4**, 737–741 (2008).
29. C. Bradley, D. & E. Holloway, C. Nuclear magnetic resonance and cryoscopic studies on some alkoxides of titanium, zirconium, and hafnium. *J. Chem. Soc. A* 1316–1319 (1968) doi:10.1039/J19680001316.
30. Deringer, V. L. *et al.* Origins of structural and electronic transitions in disordered silicon. *Nature* **589**, 59–64 (2021).
31. Bhat, M. H. *et al.* Vittrification of a monatomic metallic liquid. *Nature* **448**, 787–790 (2007).
32. Hunt, N. T., Turner, A. R., Tanaka, H. & Wynne, K. The Ultrafast Dynamics of Hydrogen-Bonded Liquids: Molecular Structure-Dependent Occurrence of Normal Arrhenius or Fractional Stokes–Einstein–Debye Rotational Diffusive Relaxation. *J. Phys. Chem. B* **111**, 9634–9643 (2007).
33. Perticaroli, S. *et al.* Structural relaxation, viscosity, and network connectivity in a hydrogen bonding liquid. *Phys. Chem. Chem. Phys.* **19**, 25859–25869 (2017).
34. Gallo, P. *et al.* Water: A Tale of Two Liquids. *Chem. Rev.* **116**, 7463–7500 (2016).
35. Yue, Y. & Angell, C. A. Clarifying the glass-transition behaviour of water by comparison with hyperquenched inorganic glasses. *Nature* **427**, 717–720 (2004).
36. Turton, D. A. *et al.* Terahertz underdamped vibrational motion governs protein–ligand binding in solution. *Nat. Commun.* **5**, 3999 (2014).
37. Neese, F. The ORCA program system. *WIREs Comput. Mol. Sci.* **2**, 73–78 (2012).
38. Bannwarth, C., Ehlert, S. & Grimme, S. GFN2-xTB—An Accurate and Broadly Parametrized Self-Consistent Tight-Binding Quantum Chemical Method with Multipole Electrostatics and Density-Dependent Dispersion Contributions. *J. Chem. Theory Comput.* **15**, 1652–1671 (2019).
39. Perdew, J. P., Burke, K. & Ernzerhof, M. Generalized Gradient Approximation Made Simple. *Phys. Rev. Lett.* **77**, 3865–3868 (1996).
40. Yanai, T., Tew, D. P. & Handy, N. C. A new hybrid exchange–correlation functional using the Coulomb–attenuating method (CAM-B3LYP). *Chem. Phys. Lett.* **393**, 51–57 (2004).
41. Grimme, S., Antony, J., Ehrlich, S. & Krieg, H. A consistent and accurate ab initio parametrization of density functional dispersion correction (DFT-D) for the 94 elements H–Pu. *J. Chem. Phys.* **132**, 154104 (2010).
42. Grimme, S., Ehrlich, S. & Goerigk, L. Effect of the damping function in dispersion corrected density functional theory. *J. Comput. Chem.* **32**, 1456–1465 (2011).
43. Weigend, F. & Ahlrichs, R. Balanced basis sets of split valence, triple zeta valence and quadruple zeta valence quality for H to Rn: Design and assessment of accuracy. *Phys. Chem. Chem. Phys.* **7**, 3297–3305 (2005).
44. Barone, V. & Cossi, M. Quantum Calculation of Molecular Energies and Energy Gradients in Solution by a Conductor Solvent Model. *J. Phys. Chem. A* **102**, 1995–2001 (1998).
45. Caughlan, C. N., Smith, H. S., Katz, W., Hodgson, Wm. & Crowe, R. W. Organic Compounds of Titanium. II. Association of Organic Titanates in Benzene Solution. *J. Am. Chem. Soc.* **73**, 5652–5654 (1951).
46. Babonneau, F. *et al.* XANES and EXAFS study of titanium alkoxides. *Inorg. Chem.* **27**, 3166–3172 (1988).
47. R.L. Martin & G. Winter. Structure of the Trinuclear Titanium (IV) Alkoxides. *Nature* **188**, 313–315 (1960).
48. Henkelman, G., Uberuaga, B. P. & Jónsson, H. A climbing image nudged elastic band method for finding saddle points and minimum energy paths. *J. Chem. Phys.* **113**, 9901–9904 (2000).
49. Bitzek, E., Koskinen, P., Gähler, F., Moseler, M. & Gumbusch, P. Structural Relaxation Made Simple. *Phys. Rev. Lett.* **97**, 170201 (2006).
50. Trygubenko, S. A. & Wales, D. J. A doubly nudged elastic band method for finding transition states. *J. Chem. Phys.* **120**, 2082–2094 (2004).
51. Sheppard, D., Terrell, R. & Henkelman, G. Optimization methods for finding minimum energy paths. *J. Chem. Phys.* **128**, 134106 (2008).

Acknowledgments

KW acknowledges funding by a grant from the European Research Council (ERC) under the European Union’s Horizon 2020 research and innovation program (grant agreement No. 832703) and the Engineering and Physical Sciences Research Council (EPSRC) for support through grant EP/N007417/1. KW and HMS acknowledge funding by Leverhulme Trust Research Project Grant RPG-2018-350. UJ and GM acknowledge financial support from the Slovenian Research Agency (project I0-0003). LH thanks the Carnegie Trust for a Carnegie Vacation Scholarship. We acknowledge the University of Glasgow for funding, and the award of a College of Science and Engineering PhD Scholarship to Tajrian Chowdhury. We gratefully thank Dr. Nicolás Flores-González for preparing a titanium ethoxide ssNMR sample under argon. Last but certainly not least, KW is extremely grateful for Paul McMillan for extensive discussions and encouragement during the Covid lockdown period up until his untimely death on 2 February 2022, which led to a revisitation of all the fundamentals of glass science and reconsideration of everything afresh.

Author contributions

All authors contributed to the study and manuscript. BAR assisted by LH and MT carried out the calorimetry, Raman spectroscopy, and rheology. NVT and HMS were responsible for the quantum chemistry calculations of molecular structures, transitions states, and spectra. MGJ performed the OKE experiments. TC and JF were responsible for synthesis. UJ and GM were responsible for the MAS NMR measurements. BAR and KW carried out data analysis and manuscript preparation.

Competing interests

The authors declare no competing interests.

Additional information

Additional information is linked to the online version of the paper at www.nature.com/nature.

Corresponding author

Klaas Wynne – University of Glasgow, School of Chemistry, Glasgow G12 8QQ, UK; email: klaas.wynne@glasgow.ac.uk.

Supplementary information

Supplementary tables

Supplementary Table 1. Calorimetric glass transition temperatures and heat capacity changes of the high temperature glass transition only. DSC data obtained using controlled cooling to ~190 K and heating at 10 K/min. DSC data are in Fig. 2.

	M_{monomer} / g mol ⁻¹	$M_{\text{effective}}$ / g mol ⁻¹	T_{g1} / K	ΔC_{p1} / JK ⁻¹ mol ⁻¹	T_{g2} / K	ΔC_{p2} / JK ⁻¹ mol ⁻¹
Titanium ethoxide	228.15	684.45	-	-	230.7	222.4
Titanium propoxide	284.22	852.66	-	-	237.3	219.1
Titanium butoxide	340.32	1020.96	-	-	233.7	327.7
Titanium 2-ethylhexyloxyde	564.75	1694.25	-	-	226.7	867.5
Niobium butoxide	458.12	916.24	-	-	n/a	n/a
Titanium 2-ethylhexanoate	623.75	623.75	-	-	n/a	n/a

Supplementary Table 2. Calorimetric glass transition temperatures and heat capacity changes of both glass transitions. DSC data obtained using quench cooling to ~120 K and heating at 20 K/min. DSC data are in Fig. 2.

	M_{monomer} / g mol ⁻¹	$M_{\text{effective}}$ / g mol ⁻¹	T_{g1} / K	ΔC_{p1} / JK ⁻¹ mol ⁻¹	T_{g2} / K	ΔC_{p2} / JK ⁻¹ mol ⁻¹	$\Delta C_{p,\text{total}}$ / JK ⁻¹ mol ⁻¹
Titanium ethoxide	228.15	684.45	189.2	103.4	240.4	180.0	283.4
Titanium propoxide	284.22	852.66	176.6	163.7	245.8	289.1	452.8
Titanium butoxide	340.32	1020.96	162.1	222.6	243.2	232.8	455.3
Titanium hexoxide	442.46	1327.368	164.0	512.4	245.8	351.8	864.2
Titanium 2-ethylhexyloxyde	564.75	1327.38	179.7	404.9	234.2	648.9	1053.8
Niobium butoxide	458.12	1129.5	154.0	260.5	n/a	n/a	n/a
Titanium 2-ethylhexanoate	623.75	623.75	182.0	142.2	n/a	n/a	n/a

Supplementary Table 3. Fits to the temperature-dependent shear viscosity using a Vogel-Fulcher-Tammann function. The function used is $\eta = \eta_0 \exp(D/(T - T_0))$. The data below and above 230 K (-40°C) were fitted separately as described in the main text. The fits are shown in Fig. 3 and Supplementary Figure 5.

	η_0 (low T) / Pa·s	D (low T) / K	T_0 (low T) / K	η_0 (high T) / Pa·s	D (high T) / K	T_0 (high T) / K
Titanium propoxide	0.0006±0.0001	1319±18	135.3±0.4	0.013±0.002	330±19	202.9±1.5
Titanium butoxide	0.0041±0.0005	857±15	129.2±0.5	0.00025±0.00002	819±15	156.3 ± 1.1
Titanium hexoxide	0.0082±0.0007	727± 9	134.7±0.3	5.7 10 ⁻⁶ ±4.2 10 ⁻⁵	1236±1.6 10 ³	152±68
Titanium 2-ethylhexyloxyde	0.008±0.003	1062±46	137.9±1.2	8.9 10 ⁻⁵ ±1.4 10 ⁻⁵	947±30	170.1±1.4
Niobium butoxide	0.0014±0.0001	811±13	123.2±0.4	n/a	n/a	n/a
Titanium 2-ethylhexanoate				n/a	n/a	n/a

Supplementary Table 4. Energies (relative to the most stable isomer) for the isomers I–V of Ti(OR)₄ trimers (R = Me, Et, n-Bu) shown in Supplementary Figure 9 as obtained by PBE0-D3(BJ)/def2-TZVPP,CPCM(n-hexane).

kJ/mol	I	II	III	IV	V
Me					
ΔE	19.6	15.0	0.0	12.1	30.5
ΔH_{298}	19.2	18.8	0.0	13.4	32.2
ΔG_{298}	17.6	28.4	0.0	6.3	32.6
Et*					
ΔE	18.8	23.0	0.0	2.5	32.6
n-Bu*					
ΔE	30.5	0.0	0.8	5.0	20.9

* PBE0-D3(BJ)/def2-TZVPP values for ethoxides and butoxides correspond to structures resulted from geometry optimization; Hessians for these structures were not computed.

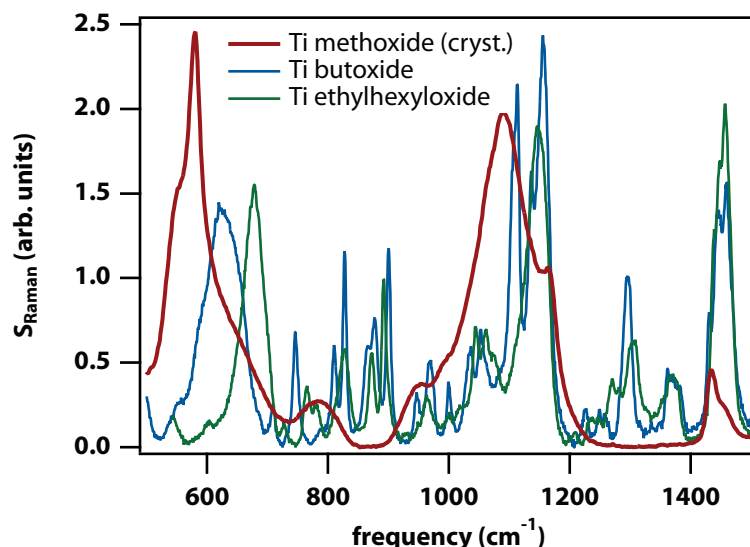
Supplementary Table 5. Energies (in kJ/mol, relative to the lowest-energy isomer at each level) for titanium ethoxide trimers estimated in chloroform (ALPB solvation model for GFN2-xTB and CPCM for DFT and ab initio).

	I	II	III	IV	V
GFN2-xTB	40.1	2.9	0.0	5.9	40.5
DFT	46.9	20.1	11.7	0.0	57.8
MP2	38.8	8.6	0.3	0.0	54.1
CCSD	37.7	18.9	13.9	0.0	55.3
CCSD(T)	38.3	10.9	7.4	0.0	52.3

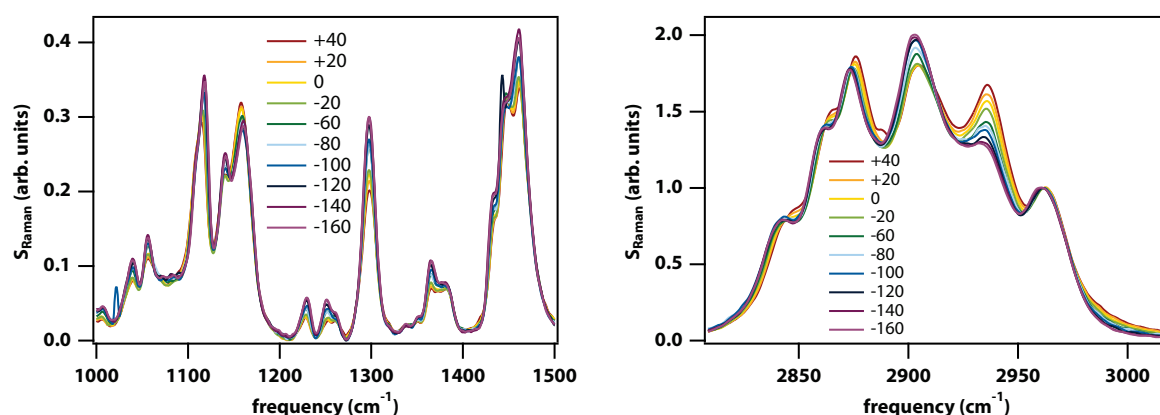
Supplementary Table 6. Highest barriers (in kJ/mol) on the isomerisation pathway estimated by GFN2-xTB method (ALPB, chloroform). Values correspond to transitions from the skeleton indicated in the corresponding column (left) to skeleton in the row (top).

	I	II	III	IV	V
I	-	77.8	73.7	32.9	35.9
II	114.8	-	21.5	137.2	132.2
III	113.7	24.6	-	113.1	137.5
IV	67.2	134.6	107.3	-	68.0
V	35.3	94.5	96.7	33.0	-

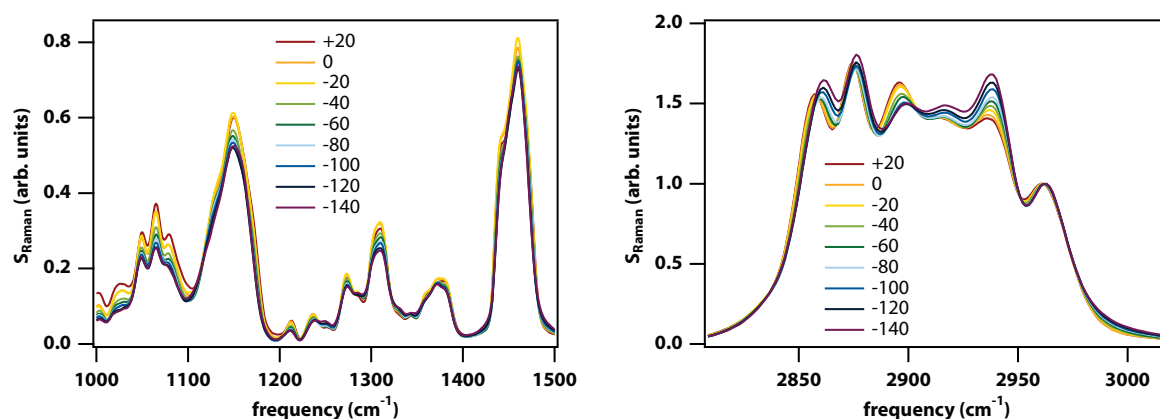
Supplementary figures – Raman spectra



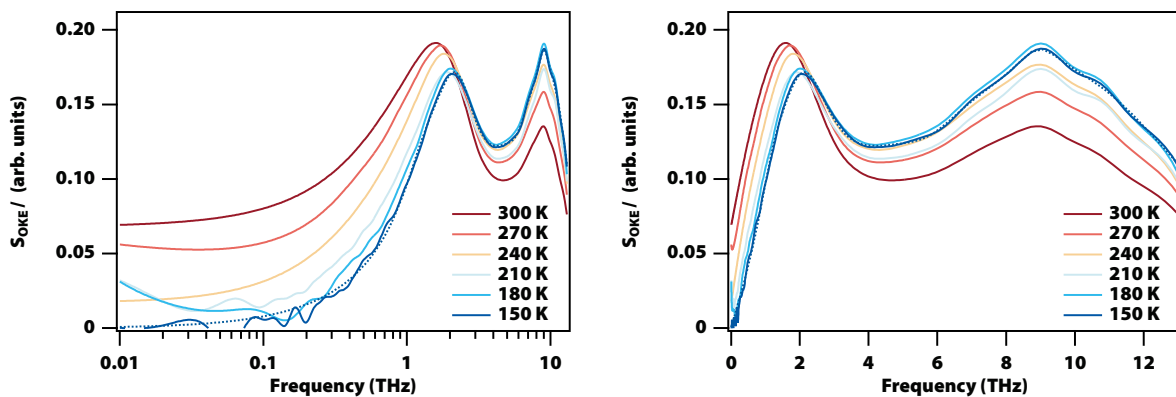
Supplementary Figure 1. Room temperature Raman spectra of crystalline titanium methoxide and liquid titanium butoxide and 2-ethylhexyloxide in the 500–1,500 cm^{-1} region. The spectrum of titanium methoxide is relatively simple due to the strict octahedral coordination of the titanium atoms in the tetrameric crystalline state. The spectra of titanium butoxide and 2-ethylhexyloxide are much more complicated due to a mixture of coordination numbers in the trimeric liquid.



Supplementary Figure 2. Temperature-dependent Raman spectra of titanium butoxide. (left) The fingerprint region and (right) the CH-stretch region. The spectra have been normalised at 2961.5 cm^{-1} .

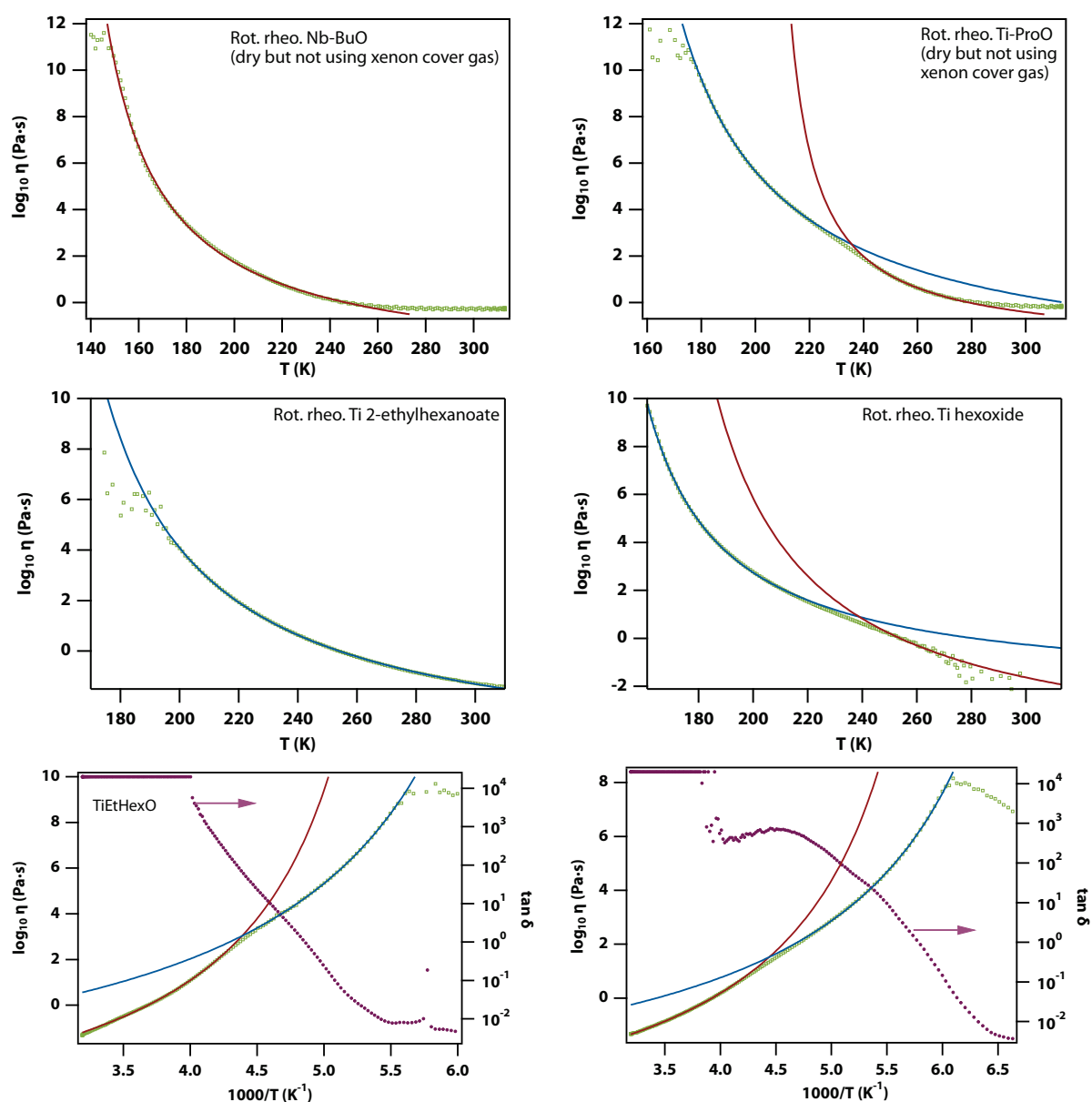


Supplementary Figure 3. Temperature-dependent Raman spectra of titanium 2-ethylhexyloxide. (left) The fingerprint region and (right) the CH-stretch region. The spectra have been normalised at 2961.5 cm^{-1} .



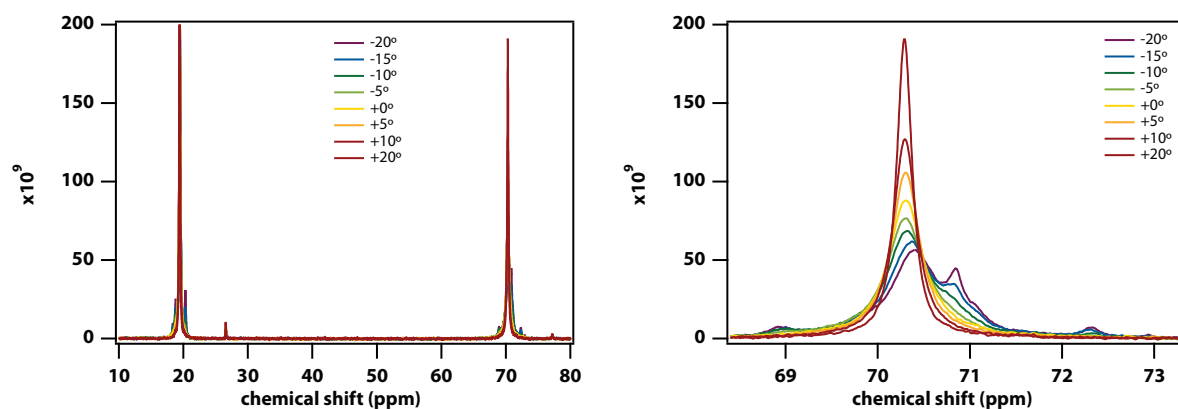
Supplementary Figure 4. Optical Kerr-effect (OKE) spectra of supercooled and vitrified titanium 2-ethylhexyloxyde. Data from 150 to 300 K (solid lines) and fit to multiple Brownian oscillator (Lorentzian) functions for the 150 K spectrum (dotted). The two lowest frequency bands have central frequencies of 1.08 ± 0.05 THz and 1.8 ± 0.2 THz.

Supplementary figures – Rheology

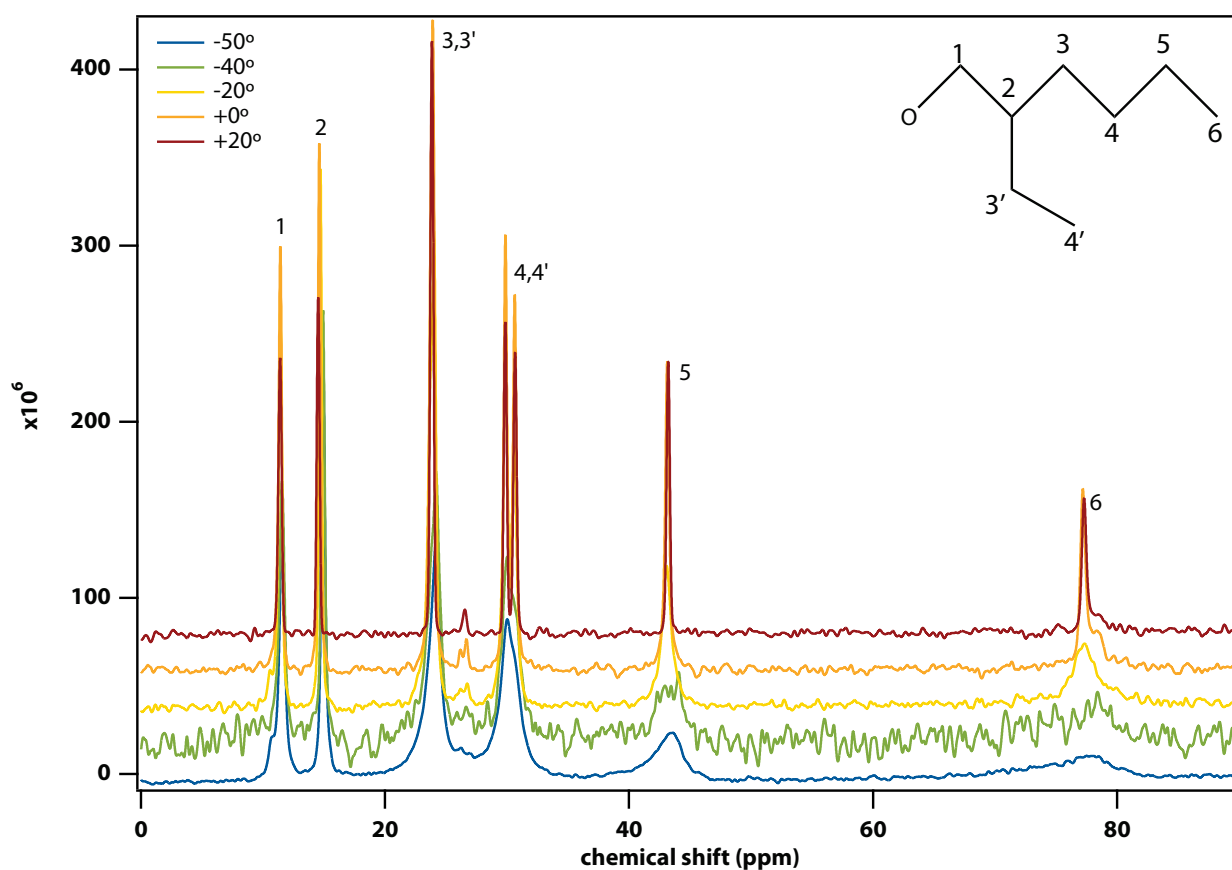


Supplementary Figure 5. Shear viscosity measurements of a number of transition-metal alkoxides. Shown are data for niobium butoxide, titanium propoxide, titanium 2-ethylhexanoate, and titanium hexoxide on a normal temperature scale. Also shown are the data and fits from Fig. 3 on an inverted temperature scale.

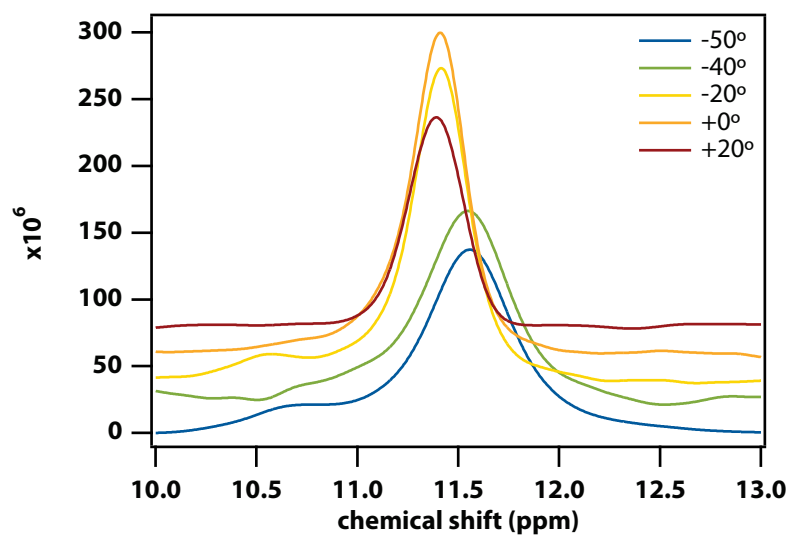
Supplementary figures – ^{13}C ssNMR



Supplementary Figure 6. ^{13}C MAS NMR spectra of titanium ethoxide. Temperatures -20, -15, -10, -5, 0, 5, and 10°C. The lines near 70 ppm are due to the CH₂ group in titanium ethoxide while those near 20 ppm are due to the terminal methyl group.

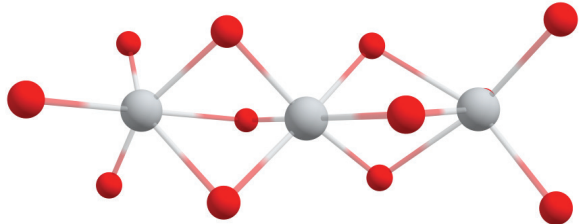
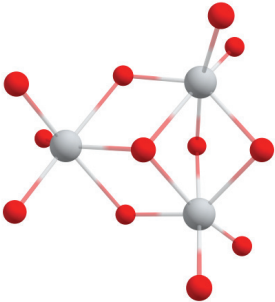
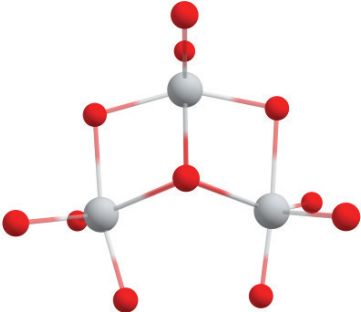
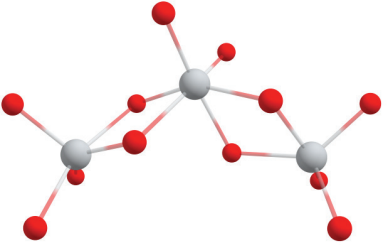
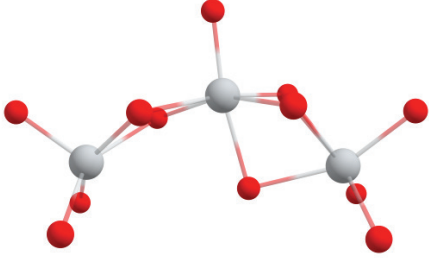


Supplementary Figure 7. ^{13}C MAS NMR spectra of titanium 2-ethylhexyloxide. Temperatures -50, -40, -20, 0, and 20°C.

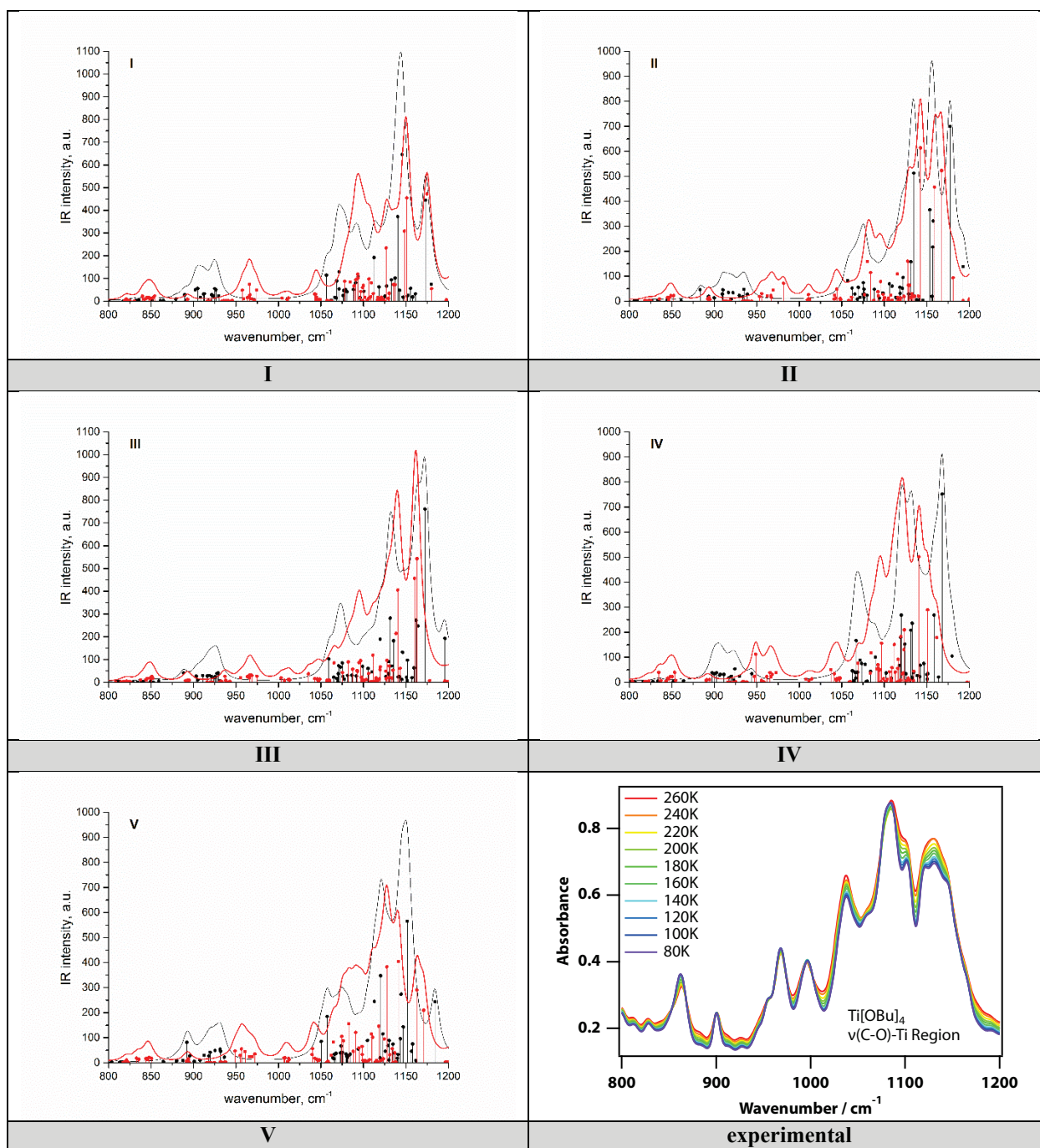


Supplementary Figure 8. ¹³C MAS NMR spectra of titanium 2-ethylhexyloxide. Temperatures -50, -40, -20, 0, and 20°C. A shift due motional narrowing occurs between -20° and -40°C consistent with an activation energy of 46 ± 2 kJ/mol.

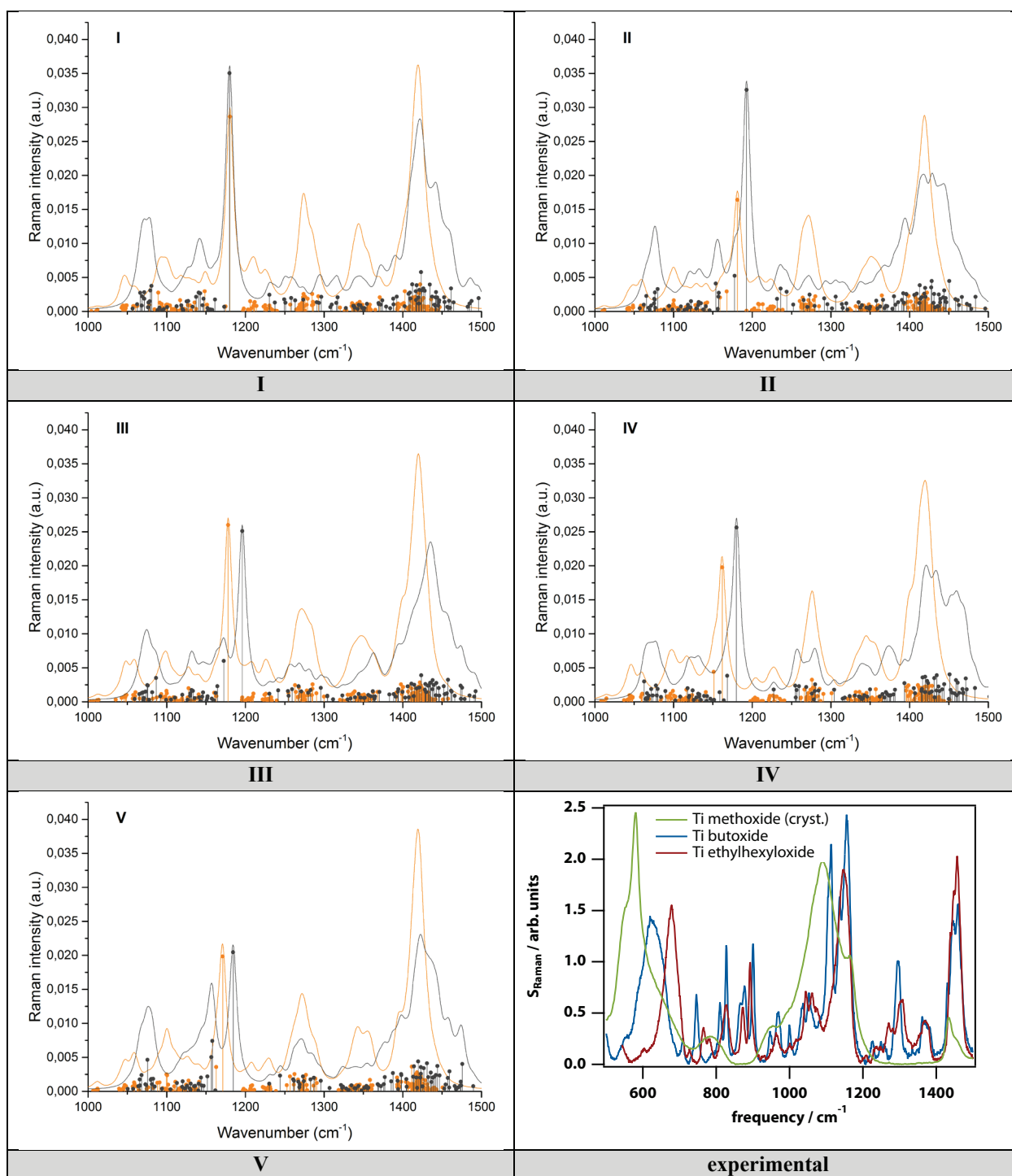
Supplementary figures – Conformer stability, normal-mode, and spectral calculations

	<ul style="list-style-type: none"> • 3 distorted TiO₆ octahedra connected face-to-face such that the Ti–Ti–Ti angle is close to 180° (2 shared faces) • 6 μ_2 and 6 terminal oxygens • S₆ point symmetry group
<p>I</p> 	<ul style="list-style-type: none"> • 2 distorted TiO₆ octahedra connected face-to-face + TiO₆ octahedron sharing 2 edges with each of these two • 1 μ_3, 4 μ_2 and 7 terminal oxygens • C_s point symmetry group
<p>II</p> 	<ul style="list-style-type: none"> • 3 distorted TiO₆ octahedra connected face-to-face with each other (3 shared faces) • 2 μ_3, 2 μ_2 and 8 terminal oxygens • C₂ point symmetry group
<p>III</p> 	<ul style="list-style-type: none"> • 1 distorted TiO₆ octahedron sharing 2 edges with 2 square-pyramidal TiO₅ • 4 μ_2 and 8 terminal oxygens • C₂ point symmetry group
<p>IV</p> 	<ul style="list-style-type: none"> • 2 distorted TiO₆ octahedra connected face-to-face + 1 TiO₅ square pyramid sharing an edge with the “central” TiO₆ • 5 μ_2 and 7 terminal oxygens • C_s point symmetry group
<p>V</p>	

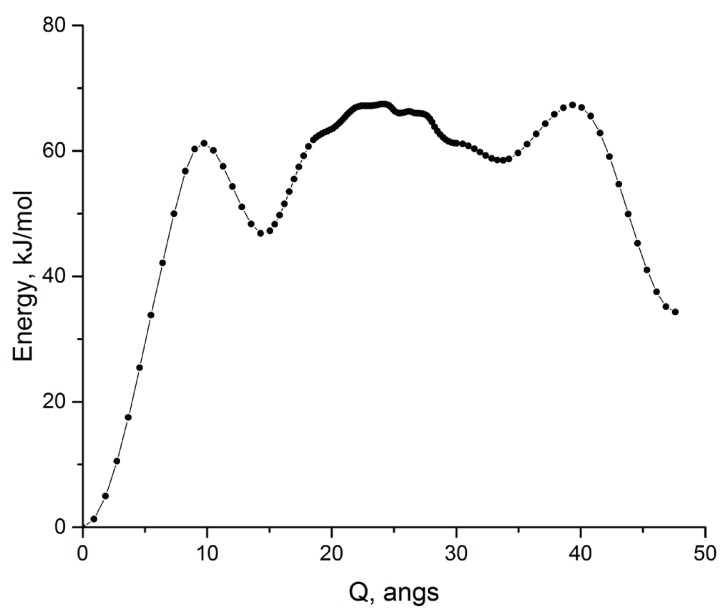
Supplementary Figure 9. Ti₃O₁₂ cores for different isomers of Ti(OR)₄ trimers (R = Me, Et, n-Bu).



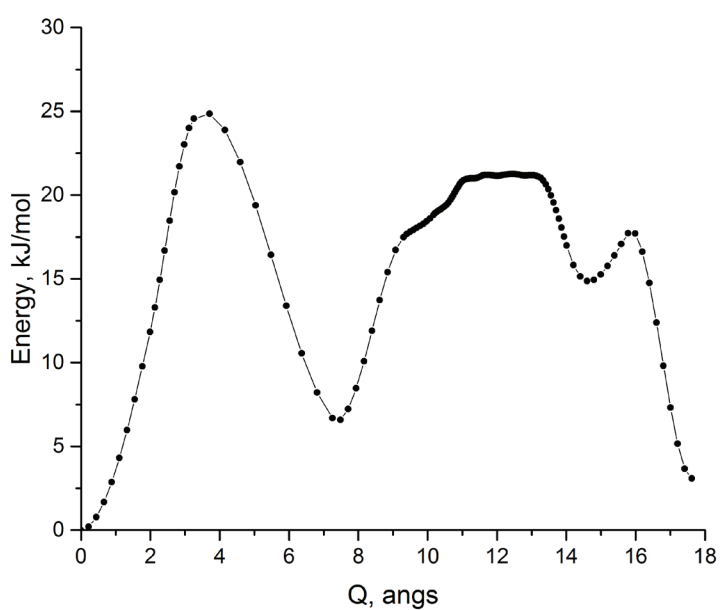
Supplementary Figure 10. Computed and experimental spectra of titanium butoxide in the mid-IR. This region shows bands due to C-O-Ti stretching/bending modes. Theoretical spectra computed by PBE/def2-SVP for different Ti(OR)₄ trimers (R = Et (black), n-Bu (red)).



Supplementary Figure 11. Computed and experimental Raman spectra of titanium alkoxides in 1000-1500 cm^{-1} region. This region shows bands due to C-O-Ti stretching/bending modes. Theoretical spectra computed by PBE/def2-SVP for different $\text{Ti}(\text{OR})_4$ trimers (R = Et (dark grey), n-Bu (orange)).



IV-I



III-II

Supplementary Figure 12. Estimated (Zoom-NEB-CI) minimal energy paths for IV-I and III-II transitions on GFN2-xTB PES. 116 images were generated during Zoom-NEB-CI procedure for IV-I transition and 125 for III-II transition (not including end points). Intermediate minima correspond to processes involving alkyl chains rotations.

Supplementary notes

Supplementary note 1

Bloch-McConnell vs. translational diffusion

The Bloch-McConnell equation describes the merging of two NMR spectral lines due to rapid exchange with rate k . The frequencies are given by

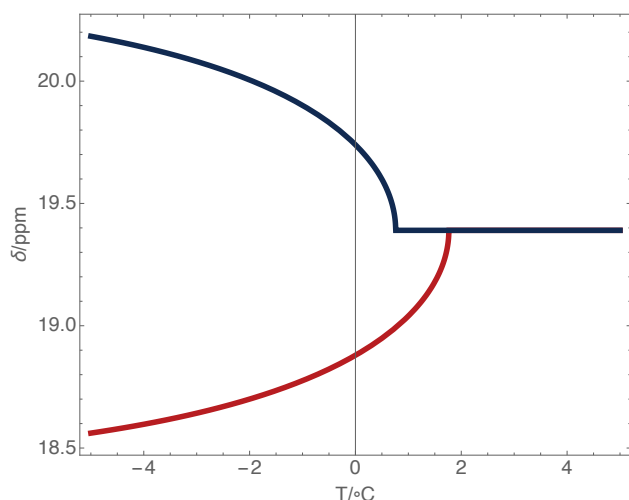
$$\omega_{\pm} = \frac{1}{2}(\omega_1 + \omega_2) \pm \text{Re} \sqrt{\frac{1}{4}(\omega_1 - \omega_2)^2 - k^2},$$

where ω_1 and ω_2 are the angular frequencies of the peaks of the unperturbed lines, and ω_{\pm} are the angular frequencies with the exchange.

It would be reasonable to assume that the rate of ligand exchange is activated and described by an Arrhenius equation. However, the Arrhenius equation has two parameters, which would be difficult to determine over the limited accessible temperature range. Therefore, an Eyring expression

$$k = \frac{k_B T}{h} \exp\left(-\frac{E_B}{RT}\right)$$

was used where E_B is an activation enthalpy to be determined through fitting to the data and it is assumed that the change in entropy can be ignored. The temperature at which two lines merge is a very strong function of the barrier energy as can be seen in Supplementary Figure 13.



Supplementary Figure 13. Calculated upper and lower NMR peak shift for barrier heights of 52.2 kJ/mol (upper) and 52.4 kJ/mol (lower). The value 52.3 kJ/mol is used in Fig. 4.

A translational relaxation rate is calculated using the Stokes-Einstein equation for the translational diffusion coefficient

$$D_T = \frac{k_B T}{6\pi\eta R},$$

where η is the viscosity and R the molecular radius, which is calculated from the molecular mass m and liquid density ρ as

$$R = \sqrt[3]{\frac{3}{4\pi} \frac{m}{\rho N_A}},$$

where N_A is Avogadro's number. The time for diffusion over one molecular diameter is given by

$$\tau_T = \frac{(2R)^2}{6D_T},$$

which gives a diffusion rate of

$$k_T = \frac{k_B T}{4\pi R^3 \eta}.$$

Supplementary note 2

Calculation of stable structures of titanium alkoxides

A search for stable conformers was carried out as described in the Methods section. Among the predicted structures (see Supplementary Figure 9), for I-III the coordination number for all titanium atoms is 6, and for other two, either one (V) or two (IV) titanium atoms are coordinated by 5 oxygens. It is important to stress, however, that in all these structures, the TiO_6 and TiO_5 cores are notably distorted: they do not form perfect octahedra nor trigonal bipyramids. One can imagine structures I-III and V formed from a dimer of TiO_6 octahedra stacked face to face, adding a third one in such a way as to form a linear chain (I) or to have two adjacent edges and one common vertex (II) or, finally, to have three shared faces and two common vertices (III); V is formed by adding a trigonal bipyramid sharing one edge. Structure IV is comprised of distorted TiO_6 octahedron with two trigonal TiO_5 bipyramids attached.

The structures predicted here are at variance with the conclusions of Ref. ⁴⁶ based on XANES/EXAFS data, that the stable structure in the liquid phase has all three titanium atoms with 5-fold (D_{3h}) coordination. We believe that this discrepancy can be attributed to the aforementioned distortions from ideal TiO_6 octahedral coordination characteristic for all structures predicted here; for example, for the terminal TiO_6 "octahedron" in structure I, the TiO distances range from 1.78 to 2.35 Å. As a result, the coordination is probably more difficult to establish experimentally for these clusters compared to "simpler" complexes. It is easy to see that all these structures possess somewhat different local environments for oxygens (see Fig. 9) and therefore NMR ^{17}O data could be helpful in identifying the correct conformer(s) in solution.

Relative energies, enthalpies and Gibbs free energies of the predicted structures are presented in Supplementary Table 4. Generally, structure V is among the highest in energy and is therefore least likely to be observed in solution. For titanium methoxide, it seems safe to assume that conformer III is dominant in solution. For titanium ethoxide, energy differences between structures III and IV are relatively small, and the correct ordering is beyond the accuracy of theory. It is likely that both these structures are present in comparable amount in solution. In previous work¹⁷ it was proposed on the basis of B3LYP/6-31G* calculations that trimers exist either in structure I or III (in our notations). While we obtain qualitatively similar trends (structure III is lower in energy, but the gap is greatly reduced if the entropy is accounted for), based on our calculations the energy difference is still notable enough to expect that structure I could be excluded from consideration as well as V.

For titanium butoxide, our calculations predict that structure II is formally the lowest in energy, and PBE0/def2-TZVPP calculations show that III and IV (to lesser extent) should be taken into account as well. Thus, the prediction here is that—unlike in the crystal phase (where it exists)—titanium ethoxide and butoxide occur as a mixture of conformers II (only for n-Bu), III, and IV. The closeness of the energies of these notably different structures combined with low barriers to conformational transitions between them might be one of the reasons behind the large fragility of the supercooled liquid and the difficulty in obtaining crystals of these compounds.

Because of the differences in local environments for the oxygen atoms, it might be possible to use vibrational spectroscopy to determine what species exist in solution. It can be shown in the case of TiEtO that enlarging the basis set (from def2-SVP to def2-TZVP) leads to a red shift and a reduction in the (absolute) intensity of the vibrational spectra. However, the relative intensities are similar and therefore def2-SVP should provide a reasonable picture for qualitative conclusions at a reduced computational cost. However, the IR spectra of the different structures of TiBuO in the CO-stretch region (from approximately 950 to 1250 cm⁻¹, see Supplementary Figure 10) are not sufficiently different to make a definitive assignment as to which structure is most prevalent in the liquid phase.

Supplementary note 3

Isomerisation energies of titanium alkoxides

In order to assess the viability for titanium alkoxides to interconvert between the isomers I–V, we estimated the corresponding energy barriers. First, 5 structures exemplifying 5 different TiO skeletons were selected (from the previously studied 50 conformers, see above) and optimised on semiempirical GFN2-xTB level, and then with PBE-D3(BJ)/def2-SVP with CPCM(chloroform) solvation model. To assess DFT accuracy, DLPNO-MP2/cc-pVTZ and DLPNO-CCSD(T) single point calculations in cc-pVTZ basis set were carried out on top of DFT geometries. From the 50 structures found (see above), the structure with the lowest energy was chosen. Then, simple deformations (e.g. ‘linearizing’ Ti-Ti-Ti angle to get to the structure I) were applied followed by GFN2-xTB geometry optimizations. This approach was utilized to get 5 isomers that were located relatively close to each other PES-wise. Since we aim to find saddle points characteristic to transitions between isomers, we would like to receive a shorter reaction path with fewer barriers. Because of that, 5 structures studied in the present supplementary section do not exactly coincide with the lowest-energy conformers for each isomer that we found before.

In the main part, we used CPCM (hexane) as a solvation model to estimate, say, conformer energy differences. Provided the information on dielectric constant for Ti(OEt)₄ is not available, it might have been interesting to see how PES would change after a relatively small increase in dielectric constant. Hence, these 5 structures were further optimized with PBE-D3(BJ)/def2-SVP with CPCM(chloroform) solvation model. Upon visual inspection of the resulted structures, it was confirmed that trimers skeletons were moderately sensitive to the increase in polarity of the medium geometry-wise and more so energy-

wise. It should be noted though that the qualitative considerations for energy ordering of isomers are not affected by the choice of a solvent – at least within PCM solvation model. Thus, to assess DFT accuracy this time, DLPNO-MP2/cc-pVTZ and DLPNO-CCSD(T) single point calculations in cc-pVTZ basis set were carried out on top of DFT geometries.

Corresponding relative energies are presented in Supplementary Table 5. Having in mind the accuracy of the methodologies used, one can see that these methods agree reasonably well predicting structures II, III and IV to be lower in energy (all within 5 kcal/mol window irrespective of the method used), while structures I and V are notably higher. This qualitative result allows us to use the xTB method in search of highest energy saddle point on minimal energy paths corresponding to all 10 possible transitions.

In order to obtain an estimate of the reaction path connecting any two isomers and the highest barrier on that path, we performed climbing image NEB (NEB-CI) calculations. We used the Zoom-NEB-CI method⁴⁷ along with the FIRE optimiser⁴⁸ and the DNEB approximation.^{49,50} To ensure tighter convergence to the actual saddle point, the maximum force acting on the CI was converged to 2×10⁻⁴ Hartree/Bohr and the RMS force to 10⁻⁴ Hartree/Bohr. Resulting MEPs usually have a few intermediate minima due to alkyl chains being obviously involved in the isomerisation process; the number of images created in Zoom variant usually exceed 100 (e.g., Supplementary Figure 12). From the viewpoint of TiO skeleton rearrangements, all corresponding processes are relatively simplistic—for instance, IV–I involves the increase of Ti–Ti–Ti angle with subsequent formation of two new TiO bonds, or for II–III 2 TiO bonds for 2 distorted octahedra with shared faces break an instead new 2 TiO bonds are formed so that previous octahedra share faces with the third one (not just edges).

— however, due to presence of radicals with flexible dihedrals, prediction of the “exact” path becomes too complicated even on semiempirical PES (see). Values of highest energy saddle points obtained from these calculations (that could be taken as “effective” activation energies although MEPs are quite complex, and all isomerisations are not elementary acts) are listed in Supplementary Table 6.

Analysing the data, we note that the barriers to conformational transitions between forms II and III; and forms (I, IV, V) are notably lower than those for other (say, I–II) transitions.

Supplementary note 4

Synthesis of Titanium hexoxide

General Experimental Considerations

All air-sensitive manipulations were carried out in an MBraun glovebox (O₂ < 0.1 ppm and H₂O < 0.5–1.5 ppm) or by using standard Schlenk techniques under N₂. All glassware was dried at 130–135°C overnight prior to use. An Innovative Technology Inc. Pure Solv 400-5-MD solvent purification system (activated alumina columns) was used to obtain anhydrous toluene. Anhydrous toluene was degassed, sparged with N₂, and stored in ampoules over activated 3.0-Å molecular sieves (25–35% weight by volume) under N₂. Dryness was confirmed by using a sodium benzophenone ketyl solution after 24–48 hours. Deuterated

benzene was dried by directly transferring from sealed glass ampoules onto activated 3.0 Å molecular sieves and stored in ampoules in a N₂ atmosphere glovebox. Dryness was confirmed by ¹H NMR after 48 hours. Deuterated chloroform (99.8% *d*-atom) was purchased from Cambridge Isotope Laboratories, Inc. and stored under ambient conditions and used without further purification. The following starting materials were purchased from Alfa Aesar: 1-hexanol (99% liquid) and [Ti(NMe₂)₄] (99.9% metal basis). 1-hexanol was degassed by freeze-pump-thaw degassing cycles (×5) and stored in a pencil ampoule over activated 3.0-Å molecular sieves in a N₂ atmosphere glovebox. The yellow liquid [Ti(NMe₂)₄] was stored in a pencil ampoule in a N₂ atmosphere glovebox and used without further purification.

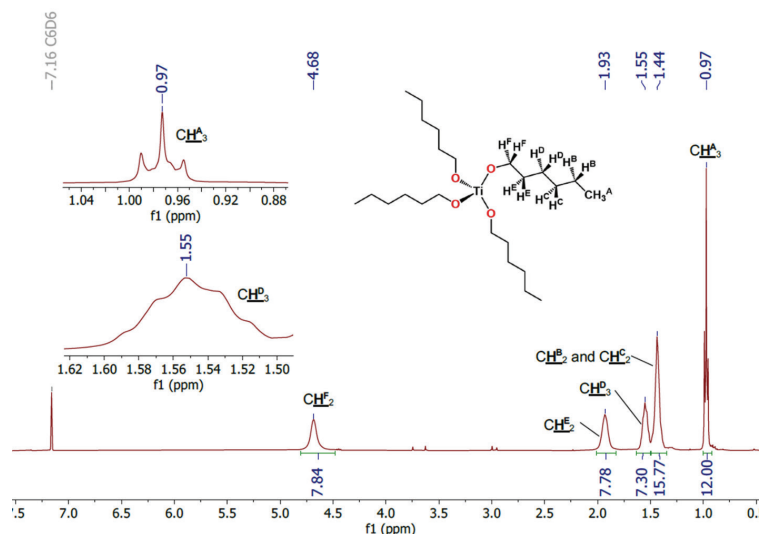
Physical Methods

¹H NMR data were recorded on an AVIII 400 MHz spectrometer operating at a frequency of 400.1 MHz and the NMR data were referenced internally to the appropriate residual proteo-solvent and reported relative to tetramethylsilane ($\delta = 0$ ppm). All spectra were recorded at a constant temperature of 25°C (298 K). Coupling constants (*J*) are reported in hertz (Hz). Standard abbreviations for multiplicity were used as follows: m = multiplet, t = triplet, d = doublet, s = singlet. For broad intensities, abbreviated as br, the full width at half-maximum intensity (FWHM) is provided in Hz. ATR-IR spectra were collected in air at ambient temperature using ThermoFisher Scientific Nicolet Summit LITE FTIR Spectrometer (containing a LiTaO₃ detector) equipped with Everest ATR. Abbreviations for the intensity of stretching frequencies were used as follows: s = strong, m = medium, w = weak. Elemental analysis was performed by Orla McCullough at the London Metropolitan University, using a Flash 2000 Organic Elemental Analyzer, Thermo Scientific analyser. The samples for the measurements were prepared using V₂O₅ (to ensure complete combustion of all complexes) in tin capsules inside an inert argon glovebox atmosphere.

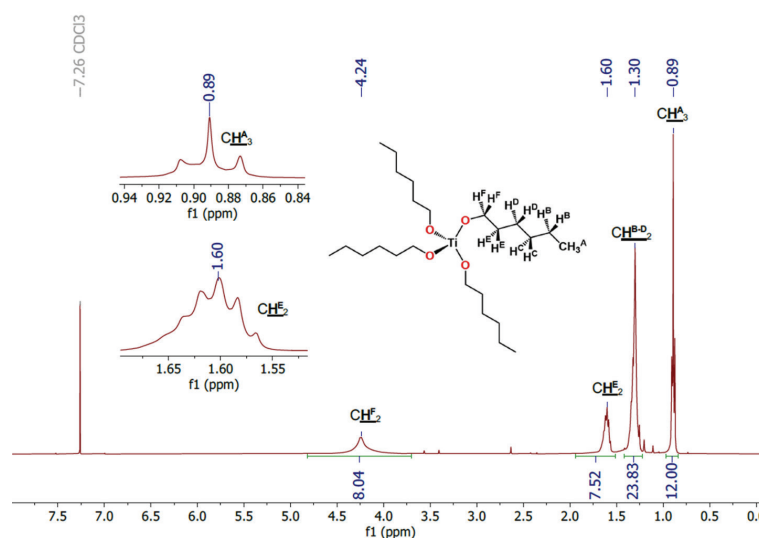
Synthesis of [Ti(OCH₂CH₂CH₂CH₂CH₂CH₃)₄] by protonolysis of [Ti(NMe₂)₄] with 4 eq of 1-hexanol

In the glovebox, a 20 mL scintillation vial was charged with a stirrer bar, and then the deep yellow liquid [Ti(NMe₂)₄] (262 μ L, 249.8 mg, 1.11 mmol, 1.0 eq) was added by a micropipette. In a separate vial, a toluene (0.5 mL) solution of the colourless alcohol 1-hexanol (556 μ L, 452.8 mg, 4.43 mmol, 4.0 eq) was prepared by weighing out the alcohol using a micropipette. To the [Ti(NMe₂)₄] liquid, the toluene solution of 1-hexanol was added, by pipette dropwise over two minutes, with stirring at ambient temperature. Dense fumes of the amine HNMe₂ were observed, and the immediate formation of a dark orange colour was noted, which was stirred at ambient temperature for an hour, after which fuming had subsided and the solution became yellow. Toluene (0.5 mL) was removed *in vacuo*, to yield a dense yellow oil, which was dried *in vacuo* (10⁻² mbar, 3.5 h) yielding [Ti(OCH₂CH₂CH₂CH₂CH₂CH₃)₄] (442.8 mg, 0.978 mmol, 88%) as a yellow oil. ¹H NMR (*d*₆-benzene): δ 0.97 (12H, t, ³*J*_{H-H} = 7.0 Hz, CH₃) 1.44 (16H, m, TiO(CH₂)₃(CH₂)₂CH₃) 1.55 (8H, approx. quintet, ³*J*_{H-H} = 7.5 Hz, TiO(CH₂)₂CH₂) 1.93 (8H, br s, FWHM = 23.3 Hz, TiOCH₂CH₂) 4.68 (8H, br s, FWHM = 22.5 Hz, TiOCH₂) ppm. ¹H NMR (*d*-chloroform): δ 0.89 (12H, t, ³*J*_{H-H} = 6.7 Hz, CH₃) 1.30 (24H, m, TiO(CH₂)₂(CH₂)₃CH₃) 1.60 (8H, approx. quintet, ³*J*_{H-H} = 6.9 Hz, TiOCH₂CH₂) 4.24 (8H, br s, FWHM = 36.6 Hz, TiOCH₂) ppm. Anal. Calcd. for C₂₄H₅₂O₄Ti: C, 63.70%; H, 11.58%; N, 00.00%. Found: C, 57.04-57.38%; H, 10.09-10.61%; N, 0.21-0.28%. Note: A small % of N is observed in the product owing to minute HNMe₂ impurities, resulting in slight discrepancies with the calculated values. Lower CHN values than calculated may be the result of incomplete combustion. However, the observed CH ratio C₂₄H₅₂ approximately matches the calculated. IR (ATR): 3070-3596 (w, ν_{OH}), * 2953 (s, ν_{sp^3-CH}), 2923 (s, ν_{sp^3-CH}), 2857 (s, ν_{sp^3-CH}), 1468 (m), 1382 (m), 1124 (s), 1089 (s), 1057 (s), 1023 (s), 921 (m), 724 (s), 643 (s, ν_{TiO}), 605 (s) cm⁻¹. *Small amount of 1-hexanol due to adventitious decomposition of the complex in the presence of atmospheric moisture while collecting ATR-IR data in air.

Nuclear magnetic resonance (^1H NMR) data for $[\text{Ti}(\text{OCH}_2\text{CH}_2\text{CH}_2\text{CH}_2\text{CH}_2\text{CH}_3)_4]$

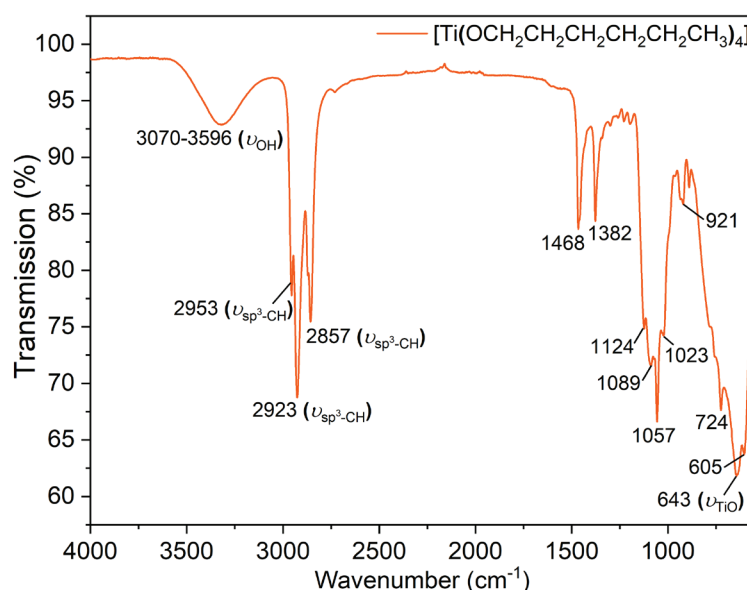


Supplementary Figure 14. ^1H NMR spectrum of $[\text{Ti}(\text{OCH}_2\text{CH}_2\text{CH}_2\text{CH}_2\text{CH}_2\text{CH}_3)_4]$, recorded in d_6 -benzene.



Supplementary Figure 15. ^1H NMR spectrum of $[\text{Ti}(\text{OCH}_2\text{CH}_2\text{CH}_2\text{CH}_2\text{CH}_2\text{CH}_3)_4]$, recorded in d_3 -chloroform.

Infrared (IR) data for $[\text{Ti}(\text{OCH}_2\text{CH}_2\text{CH}_2\text{CH}_2\text{CH}_2\text{CH}_3)_4]$



Supplementary Figure 16. ATR-IR spectrum of $[\text{Ti}(\text{OCH}_2\text{CH}_2\text{CH}_2\text{CH}_2\text{CH}_2\text{CH}_3)_4]$.